Bacterium-triggered remodeling of chromatin identifies BasR, a novel regulator of fungal natural product biosynthesis

Juliane Fischer[a,b#], Sebastian Y. Müller[c,*#], Agnieszka Gacek-Matthews[d,e], Tina Netzker[a], Nils Jäger[f], Kirstin Scherlach[g], Maria C. Stroe[a,b], María García-Altares[g], Francesco Pezzini[c,j], Hanno Schoeler[a,b], Michael Reichelt[h], Jonathan Gershenzon[h], Mario K. C. Krespach[a,b], Ekaterina Shelest[c], Volker Schroeckh[a], Vito Valiante[i], Thorsten Heinzel[f], Christian Hertweck[g,j], Joseph Strauss[d,+] and Axel A. Brakhage[a, b, +]

[a]Department of Molecular and Applied Microbiology, Leibniz Institute for Natural Product Research and Infection Biology (HKI), Beutenbergstrasse 11a, 07745 Jena, Germany

[b]Institute for Microbiology, Friedrich Schiller University Jena, Jena, Germany

[c]Systems Biology and Bioinformatics, HKI, Jena, Germany

[d]Department for Applied Genetics and Cell Biology, BOKU-University of Natural Resources and Life Sciences, Campus Tulln , Konrad Lorenz Straße 24, A-3430 Tulln/Donau, Austria

[e]Institute of Microbiology, University of Veterinary Medicine Vienna, Veterinärplatz 1, A-1210 Vienna, Austria

[f]Department of Biochemistry, Friedrich Schiller University Jena, Jena, Germany

[g]Department of Biomolecular Chemistry, HKI, Jena

[h]Department of Biochemistry, MPI for Chemical Ecology, Hans-Knöll-Str. 8, 07745 Jena, Germany

[i]Leibniz Research Group – Biobricks of Microbial Natural Product Syntheses, HKI, Jena, Germany

[j]Friedrich Schiller University Jena, Jena, Germany

[#]equal contribution

Footnotes:

*current address: Department of Plant Sciences, University of Cambridge, Downing Street, Cambridge CB2 3EA, UK

[+]corresponding authors

Axel A. Brakhage
Phone: +49 (0)3641-532 1001
Fax: +49 (0)3641-532 0802
Email: axel.brakhage@leibniz-hki.de

Joseph Strauss
Phone: +43 (0)147654-94120
Fax: +43 (0)136006-6392
Email: joseph.strauss@boku.ac.at

Key words: *Aspergillus nidulans*, histone modification, secondary metabolism, orsellinic acid, ChIP-seq, cross-pathway control, *Streptomyces rapamycinicus*, myb-like BasR, microbial interaction

Abstract

Fungi produce numerous secondary metabolites (SMs), which possess various functions *e.g.* as communication signals during coexistence with other microorganisms. Many SM biosynthesis gene clusters are silent under standard laboratory conditions because their environmental or developmental triggers are unknown. Previously, we discovered that the silent orsellinic acid (*ors*) gene cluster in the filamentous fungus *Aspergillus nidulans* is activated upon interaction with the bacterium *Streptomyces rapamycinicus* and that this induction is dependent on the GcnE lysine-acetyltransferase catalyzing histone H3 acetylation. Here, we report a genome-wide analysis of chromatin acetylation changes during this interaction and relate these to changes in the fungal transcriptome. Our results reveal that only a functional interaction with *S. rapamycinicus* changes the chromatin landscape and activates amino acid cross-pathway control in the fungus. We identified the Myb-like transcription factor BasR as novel regulator required for bacteria-triggered SM production and show that its function is conserved in other *Aspergillus* species.

Introduction

Recent advances in sequencing and mining of genomes have revealed the great potential of fungi to produce a plethora of novel secondary metabolites (SMs) (Wiemann and Keller, 2014, Macheleidt et al., 2016). These metabolites, also referred to as natural products, are low-molecular mass molecules of diverse chemical structures often with pharmacological relevance like antibiotics or cholesterol-lowering agents (Brakhage, 2013). However, the actual number of identified natural products is low when compared to the computationally identified SM gene clusters (SMCs) (Netzker et al., 2015). Many SMs are supposed to function as info-chemicals for the communication between species (Brakhage, 2013), as antimicrobials for the defense against competitors in the habitat (Keller, 2015) or as pathogenicity factors directed against host defense (Stack et al., 2007, Kazan et al., 2012). In the last decade an increasing number of studies have concentrated on fungal co-cultivation to allow for the identification of new metabolites (Scherlach and Hertweck, 2009). As an example, pestalone, an antibiotic active against methicillin-resistant *Staphylococcus aureus* and vancomycin-resistant *Enterococcus faecium*, was initially identified in a mixed fermentation of *Pestalotia* sp. and an unidentified bacterium of the genus *Thalassopia* sp. (CNJ-328) (Cueto et al., 2001). Previously, we showed that during co-cultivation of the fungus *Aspergillus nidulans* with a single bacterium identified from more than 50 species, *i.e.*, *Streptomyces rapamycinicus*, the cryptic orsellinic acid (*ors*) gene cluster was activated (Schroeckh et al., 2009). Further results indicated that the bacterium caused increased acetylation of histone H3 lysine (K) 9 and 14 at the *ors* cluster genes leading to their activation (Nützmann et al., 2011). In line, the exchange of lysine 14 to arginine, mimicking a hypoacetylated lysine residue, drastically reduced the production of orsellinic acid (Nützmann et al., 2013). The deletion of the gene coding for the lysine-acetyltransferase

(KAT also HAT) *gcnE* confirmed that the activation of the *ors* gene cluster is mediated by acetylation (Nützmann et al., 2011).

GcnE is part of the SAGA complex, which is highly conserved throughout eukaryotes. Depending on the species, SAGA consists of about 20 subunits with different functions (Baker and Grant, 2007). GcnE is responsible for the transfer of an acetyl group from acetyl-CoA to proteins like histones (Downey et al., 2015). Interestingly, GcnE of *A nidulans* is also essential for the production of the mycotoxin sterigmatocystin and the antibiotic penicillin as well as for conidiophore formation, indicating a role as global regulator of both secondary metabolism and development (Nützmann et al., 2011, Nützmann et al., 2013, Cánovas et al., 2014). The homologue for GcnE in *Saccharomyces cerevisiae* is Gcn5, which was first identified as major regulator of the cross-pathway control system. Due to its identification in a mutant (aas) sensitive against an amino acid analogue, it was originally named AAS104 (Penn et al., 1983). The fungal cross-pathway control system mediates the cross regulation of amino acid biosyntheses upon starvation for distinct amino acids (Krappmann and Braus, 2005).

The specific cross-domain microbial interaction between a eukaryotic microorganism (fungus) and a bacterium analyzed here, provides an excellent model to elucidate the underlying molecular mechanisms during microbial communication. In order to obtain a holistic view on the fungal bacterial interaction, and discover the molecular elements involved, we employed a genome-wide chromatin immunoprecipitation (ChIP) analysis during co-cultivation. This led to the discovery of major changes in the chromatin landscape triggered by the bacterium and the identification of BasR as the key regulatory node for integrating bacterial signals leading to regulation of SM gene clusters

Results

Genome-wide profiles of H3K9 and H3K14 acetylation in *A. nidulans* change upon co-cultivation with *S. rapamycinicus*

A. nidulans with and without *S. rapamycinicus* was analyzed for enrichment of acetylated (ac) histone H3 at lysines K9 and K14. For each condition, we performed ChIP-seq analyses on three independent biological replicates (Fig. 1; supplementary results) and investigated the genome-wide H3K9 and H3K14 chromatin landscape of *A. nidulans* (for details see supplementary results). The first examination of data indicated a significant proportion of co-incubated library reads (~ 80 %) originated from *S. rapamycinicus*. To account for those reads a fused genome containing the *A. nidulans* and the *S. rapamycinicus* genomes serving as our reference for mapping were constructed (see methods & supplemental results). By applying a fused genome we could quantify the relative library proportions which amounted to 8-17 % of H3, H3K14ac and H3K9ac as well as a staggering ~80 % for background reads of co-incubated libraries mapped to *S. rapamycinicus* (Table S1). However, the background read proportions might not necessarily reflect actual gDNA ratios of both species in the co-cultivation due to various potential biases. To examine read distribution for each library, we counted mapped reads within equally spaced bins along the fused genome for different resolutions (see methods and Fig. 1 A & B). As expected, background reads (Fig. 1 A, panel 1) were evenly distributed across the genome reflecting nonspecific targeting of particular areas. The fused genome further enabled for easily controlling of correct co-incubation since no reads should be mapping to *S. rapamycinicus* in non-co-incubated samples as can be seen in Fig. 1 in panels 2-4 (blue lines). Further, there were coverage dips in the middle of the

chromosomes (see Fig. 1 A, panels 1-5), which were most likely due to incomplete assembly around the centromers masked by long 'N' stretches (Ekblom and Wolf, 2014).

H3K14ac and H3K9ac showed a higher degree of variability across the genome compared to H3 implying a more specific regulatory dynamics by histone acetylation than through H3 localization. Some areas such as a region on the first half on chromosome 4 are particularly enriched in those marks, potentially marking distinctive chromatin domains. Since gene density also varies across the genome (Fig. 1 A panel 5), we addressed the question whether this correlates with the intensity of the investigated chromatin states. Calculated spearman correlation (for details see supplementary results) showed almost no correlation between the background and the genes. A domain particularly enriched for H3K9ac was found around the *ors* gene cluster (Fig. 2), thus supporting our previous data by Nützmann et al. (2011). The slight increase in H3K14ac at these promoters is apparently not seen because we only considered about 2 nucleosomes (Fig. 2) in contrast to the whole promoter areas in Fig. 1. However, the distribution of H3K14ac clearly changed during co-cultivation as seen in the IGB genome browser screen shot (Fig. 1 C) which visualizes the specific location of acetylations and histone H3 in this cluster. Again, increase of H3K9ac intensity was more pronounced than H3K14ac, although also clearly detectable, compared to modifications at genes, which are not induced by the streptomycete with particularly strong enrichment of both modifications at the *orsD* promoter. Unmodified H3 is strongly depleted throughout the cluster, especially at the *orsA* and *orsD* translation start sites (TSS).

Chromatin profiles at translation start sites and translation termination sites

Having analyzed the genome-wide distribution we next set out to assess the location of H3K9ac, H3K14ac and histone H3 relative to promoters and gene bodies by plotting the

average read count frequency for all genes to either the TSS or the translation termination site (TTS) (Fig. 3 A and B) (Yu et al., 2015). Note, due to missing information about the 5' and 3' transcriptional start and stop sites we used translation for transcription start and stop sites as surrogates. The results obtained apply to both *A. nidulans* with and without bacterium. H3K9ac and H3K14ac showed highest enrichment for the first and second nucleosomes up- and downstream of the TSS and drastic reduction downstream of the third nucleosome after the TSS (Fig. 3 A and B). Reduced occupancy of unmodified histone H3 was observed at the TSS (Kaplan et al., 2010). Towards the 3' end of genes, histone H3 occupancy gradually increased, which was accompanied by a decrease in acetylation. Plotting of differentially acetylated H3K9ac against H3K14ac showed a strong correlation between the localization of the two modifications (Fig. 4 A). Acetylation is generally described as an transcription activating mark (Gacek and Strauss, 2012). To test for this general assumption we correlated our acetylation data to microarray data generated under the same condition by Nützmann et al. (2011) (Fig. 4 B). Thereby, log-fold changes (LFCs) of the differential chromatin states were compared with the LFCs retrieved from the RNA expression data. H3K9ac correlates to the differentially expressed genes with a confidence of 0.2 in contrast to H3K14ac (-0.05) and histone H3 (-0.01) for which no detectable dependency was determined (Fig. S1, S2). To visualize the deviation of acetylation at the TSS and the TTS according to the grade of expression of the genes, we separated the differentially expressed genes into four quartiles (q1 lower 25 %, q2 the medium lower 25 – 50 %, q3 are the medium higher 50-75 %, q4 higher 25 %). The increase of acetylation at the TSS correlated with the expression level of genes (Fig. S3, S4 A & C). Decreased expression coincided with an increase of histone H3 at the TSS (Fig. S4 E).

Co-cultivation of *A. nidulans* with *S. rapamycinicus* had a major impact on SM gene clusters, nitrogen assimilation and mitochondrial activity

We employed two strategies to determine changes of histone modification levels. The first analysis was based on the finding that histone acetylation can mostly be found on histones within a gene, in particular on nucleosomes +1 and +2 (Jiang and Pugh, 2009) (Fig. 3 A). We therefore counted mapped reads in between gene boundaries for each library as basis for a quantitative comparison between mono- and co-cultivation using standard methods for sequencing data (see methods). Throughout this study, we refer to this method as differential chromatin state (DCS) analysis. The second analysis was based on a first round of peak-calling and subsequent quantification of the peaks. Comparison of the generated data sets showed 84 ± 1.7 % similarity. The data obtained from the gene-based DCS method were used for further analysis and comparison of the culture conditions using an FDR cut-off of 0.01. This does not include further filtering on the LFC to capture possible biological relevance of the detection changes. DCS analysis of H3, as a proxy for nucleosome occupancy, was found to be lower (FDR < 0.01) in four genes during co-cultivation. Using the same cut-off, H3K14ac levels were found to be lower for 154 genes and higher for 104 genes (Table 1). Most genes showed differential acetylation for H3K9ac with 297 being significantly lower and 593 being significantly higher. Gene expression according to the microarray data showed correlation with H3K9 acetylation. Therefore, a list of genes obtained from H3K9ac DCS analysis was collated showing a high correlation with gene expression. Data for a selection of genes is summarized in Table 1 showing LFCs of H3K9ac ChIP-seq with their corresponding microarray data. In total, histones belonging to six SM gene clusters showed higher acetylation including the *ors*, aspercryptin, cichorin, sterigmatocystin (*stc*), anthrones (*mdp*) and 2,4-dihydroxy-3-methyl-6-(2-oxopropyl)benzaldehyde (DHMBA) gene cluster with

the emericellamide (*eas*) cluster being the only one with reduced acetylation and expression (Table 1). Genes covered by much higher acetylated histone H3 displayed functions in calcium signaling and asexual development with a few exceptions. A major group of genes with lower acetylation is linked to the fungal nitrogen metabolism including genes for the utilization of primary and secondary nitrogen sources such as genes of the nitrate-assimilation gene cluster and the glutamine dehydrogenase gene (Fig. 5 & Fig. 6 A). These data were verified by quantifying the expression of affected genes by qRT-PCR (Fig. 6 B). The majority of the selected genes were lower transcribed in mixed cultivation compared to monoculture of *A. nidulans*. Furthermore, genes annotated with mitochondrial function showed decreased acetylation of H3K9. Constrained mitochondrial activity should alter the metabolic state of a cell. Therefore, we measured the latter in the fungus with an assay based on the reduction of resazurin to the highly fluorescent dye resorufin, which indicates the respiratory activity of a cell. The fungus alone showed a high metabolic activity, which was significantly reduced in co-cultivation (Fig. 6 C). Axenic cultivation of *S. rapamycinicus* and treatment of *A. nidulans* behaved similar to the AMM control (Fig. 6 C).

Bacteria induce the fungal cross-pathway control

A number of genes related to amino acid metabolism including the cross-pathway controlling gene *cpcA* showed increased acetylation for H3K9 during co-cultivation of *A. nidulans* with *S. rapamycinicus*. Therefore, the expression level of *cpcA* and *jlbA* (jun-like-bZIP), both highly expressed during amino acid starvation, was studied. qRT-PCR analysis showed up-regulation of *cpcA* and *jlbA* upon co-cultivation of the fungus with the bacterium (Fig. 7 A). These data implied that the increased expression of *cpcA* and other genes involved in amino acid biosynthesis was due to a depletion of amino acids in the cell. Therefore, we

measured the internal amino acid pool in *A. nidulans* both grown alone and with *S. rapamycinicus* (Fig. 7 C). As a control, the fungus was co-cultivated with *Streptomyces lividans*, which does not induce the *ors* gene cluster. As shown in Fig. 7C, significantly reduced levels of glutamine, histidine, phenylalanine, asparagine, threonine and reduced metabolism of arginine, which was supplemented to the medium, were observed. The monoculture of *A. nidulans,* a co-cultivation of *A. nidulans* with *S. lividans* as well as the addition of *S. rapamycinicus* after 24 h of fungal cultivation served as controls. All of the controls showed similar amino acid levels. Subsequently, we tested whether orsellinic acid production can be artificially induced *via* the addition of the histidine analogon 3-aminotriazole (3-AT), which is known to induce the cross-pathway control by amino acid starvation. As shown in Fig. 7 B, addition of 3-AT to *A. nidulans* monoculture led to production of orsellinic and lecanoric acid.

The transcription factor BasR is the central regulatory node of bacteria-triggered SM gene cluster regulation

The lack of a transcription factor-encoding gene in the *ors* gene cluster and the deregulation of amino acid biosynthesis during the interaction indicated that transcription factors of the cross-pathway control system, such as *cpcA*, might be involved in regulation of the *ors* gene cluster. However, deletion of the *cpcA* gene in *A. nidulans* showed no effect on the induction of the *ors* gene cluster in response to *S. rapamycinicus* (Fig. S5). Further transcription factors found in *S. cerevisiae* to be involved in amino acid regulation are Bas1 and Bas2 (Springer et al., 1996, Valerius et al., 2003). Two genes were identified in the *A. nidulans* genome (*AN7174 & AN8377*) encoding putative orthologues of the *S. cerevisiae bas1* (Fig. S6). Both genes code for Myb-like transcription factors whose function in filamentous fungi is

unknown. For *bas2* there seems to be no existing orthologue in *A. nidulans*. We compared the H3K9 acetylation and gene expression of both genes upon co-cultivation. As the gene *AN7174* showed higher H3K9 acetylation (LFC = 0.6) and drastically increased transcription (LFC = 57.8) in response to the bacterium, we decided to use it for further analyses and named it *basR*. A *basR* deletion strain was generated by replacing the ORF of *basR* with the *argB* cassette (Fig. S7 A). Expression of selected *ors* genes in the deletion strain compared to the wild–type strain was analyzed by qRT-PCR analysis (Fig. 8 A). In the *basR* deletion mutant, the *ors* genes were not activated by the bacterium, which was also illustrated by the lack of production of both orsellinic and lecanoric acid (Fig. 8 B). While the addition of 3-AT to monocultures of *A. nidulans* led to the production of orsellinic acid and derivatives thereof, the *basR* deletion mutant strain did not produce orsellinic acid upon addition of 3-AT (Fig. 7 B). Inspection of the *basR* mutant on agar plates did not reveal further obvious phenotypes (data not shown). To further substantiate the influence of *basR* on the *ors* gene cluster we generated a *basR* overexpression strain (Fig. S7 B) using the inducible tet^{On} system (Helmschrott et al., 2013). Addition of doxycyline to the media induced *basR* expression as well as the expression of the *ors* gene cluster. Consistently, orsellinic and lecanoric acid were detected by HPLC analysis (Fig. 8 B). To address the question whether other SM biosyntheses are regulated by BasR we searched for other metabolites. Obvious candidates were the emericellamides, as the acetylation of the corresponding gene cluster was decreased during co-cultivation (Table 1). This finding was perfectly mirrored when we applied MALDI-mass spectrometry (MS) Imaging which showed reduced levels of emericellamides in *basR* overproducing colonies of *A. nidulans* and in co-grown colonies compared to colonies without the streptomycete (Fig. 8 C).

BasR is functionally conserved in other fungal species

To address the question whether *basR* homologues exist in other fungi and whether potential homologues have similar functions, we analyzed fungal genomes using BlastP. Surprisingly, obvious *basR* homologues are only present in two other fungi, *i.e.*, *Aspergillus sydowii* and *Aspergillus versicolor*, but are apparently lacking in others (Fig. S6). Interestingly, in both fungi a gene cluster identical to the *ors* gene cluster of *A. nidulans* was also identified (Fig. 9 A). To analyze the function of the *A. sydowii basR* gene we overexpressed the gene in *A. sydowii* using the tet^{On} system (Fig. S8) and analyzed by LC-MS the appearance of novel masses. As shown in Figure 9 B, overexpression of *basR* led to the production of orsellinic acid derivatives. Co-cultivation of *A. sydowii* with *S. rapamcinicus* demonstrated that the fungal *ors* gene cluster is in fact also activated by the bacterium, again linking BasR with bacteria-triggered induction of orsellinic acid production.

Discussion

Chromatin landscape of *A. nidulans* defined by H3K9 and K14 acetylation

In addition to transcriptome and proteome analyses, this first analysis of the chromatin landscape of a eukaryotic microorganism influenced by a bacterium adds important information on the specific interaction between (micro)organisms. Here, we report the chromatin landscape in the fungus *A. nidulans* upon co-cultivation with *S. rapamycinicus* by genome-wide ChIP-seq analysis of acetylated histone H3 (H3K9ac, H3K14ac) and the quantification of H3. In an attempt to characterize the general distribution of nucleosomes and acetylation marks over the genome we compared the intensity of chromatin states with gene density. A lower gene density was typically found in heterochromatic regions such as

309 the centromeres and telomeres creating a repressing environment (Allshire and Ekwall,
310 2015). We found reduced H3 occupancy in heterochromatic regions indicating either
311 replacement of H3 by the centromere-specific H3, CENP-A or reduced nucleosome
312 occupancy (Smith et al., 2011, Allshire and Ekwall, 2015).
313 We observed distinct peaks for H3K9ac in *A. nidulans* grown in co-culture with *S.*
314 *rapamycinicus*. One of the areas with the highest increase in H3K9ac was the *ors* gene
315 cluster. Hence, this data nicely confirm our previous findings of increased acetylation of
316 H3K9 and H3K14 of the *ors* genes during the interaction of *A. nidulans* with the bacterium *S.*
317 *rapamycinicus* (Fig. 10). Previous ChIP qRT-PCR experiments indicated a distinct increase of
318 H3K9ac inside the cluster borders, which did not expand to neighboring genes (Nützmann et
319 al., 2011). By contrast, the H3K14ac modification seemed to be of a more global nature and
320 not exclusively confined to specific regions such as the *ors* gene cluster. These conclusions
321 were confirmed here by the pattern detected in the genome-wide ChIP data, showing no
322 spreading of H3K9ac to genes adjacent to the *ors* gene cluster which also demonstrates the
323 quality of the genome-wide ChIP data generated here. Furthermore, these results are also
324 consistent with our previous finding, showing reduced expression of SM cluster genes as a
325 consequence of lacking H3K14 acetylation (Nützmann et al., 2013). In contrast to H3K14ac,
326 H3K9ac is less uniformly distributed over the genome but only shows strong enrichment at
327 promoters of certain genes. Especially high levels of acetylation can be found at *orsA* and the
328 bidirectional promoter of *orsD* and *orsE*. This observation was recently confirmed by the
329 finding that H3ac and H3K4me3 were increased at the *orsD* gene only when the *ors* cluster
330 was transcriptionally active (Gacek-Matthews et al., 2016).
331 The number of genes within an SM cluster decorated with activating chromatin marks seems
332 to vary considerably between species and histone modifications. For example, ChIP-seq

analysis of H3K9ac in *Fusarium fujikuroi* did not show any difference in the degree of acetylation of the gibberellin and the bikaverin cluster genes (Studt et al., 2013). In the gibberellin cluster only a subset of genes showed methylation of the H3K4 residue (Wiemann et al., 2013). H3K9ac on the other hand was evenly distributed over promoter areas of PKS19, gibberellin, bikaverin and apicidin-like cluster genes (Wiemann et al., 2013). We also assessed the distribution of H3K9ac and H3K14ac as well as the C-terminus of H3 (H3Cterm) at the TSS and TTS. For H3K9, an enrichment of acetylation ~500 bp downstream of the TSS as well as immediately upstream of the TSS was observed. This was expected as similar results were obtained with an antibody targeting the acetylated N-terminus of histone H3 in *A. nidulans* (Gacek-Matthews et al., 2016) and other fungi such as *S. cerevisiae* and *Cryptococcus neoformans* (Haynes et al., 2011, Mews et al., 2014). Increased acetylation coincides with reduced levels of H3 around the TSS, which is most likely due to a depletion of nucleosomes at the promoter. The profile plots for H3K14 acetylation are similar, although not as highly enriched around the TSS as H3K9 (Fig. S3). As expected, a comparison of LFCs for both modifications showed high similarity suggesting that they are established interdependently (Gacek and Strauss, 2012, Waters et al., 2015). At the 3' end of the ORF, H3 density drastically increased accompanied by reduced levels of H3K9ac and H3K14ac (Fig. S4). Likewise, reduced acetylation at the TTS was observed in *A. nidulans* (Gacek-Matthews et al., 2016) and *S. cerevisiae* (Mews et al., 2014). It is interesting to notice, that the increase in nucleosome density directly correlated with a decrease in the gene expression rate (Fig. S4 E). Previous studies suggested a direct correlation between the presence of nucleosomes and the stalling of RNA II polymerase (Grosso et al., 2012). Thereby, the increased integration of nucleosomes behind the poly(A) site led to pausing of the RNA polymerase resulting in the termination of transcription (Grosso et al., 2012).

Increased gene expression directly correlates with histone H3K9 acetylation

Acetylation is generally regarded as an activating chromatin mark promoting transcription of eukaryotic genes (Bannister and Kouzarides, 2011). The acetylation of H3K9 and expression of genes directly correlated when we compared data from this study with microarray data obtained by Nützmann et al. (2011) (Fig. S1, S2). A similar finding was reported for other fungi (Wiemann et al., 2013). However, this was not observed for acetylation of H3K14, which could partly result from the low number of targets with this modification. By contrast, analysis of gene promoters showed a distinct increase of H3K14ac at the TSS in dependence on the average transcription level (Fig. S4 C). The low correlation between active gene transcription and acetylation at H3K14 confirmed earlier results obtained by our group. Previously, we showed that a mimicry of a hypo-acetylated lysine 14 on histone H3 drastically altered the phenotype and the expression of SM gene clusters in this strain (Nützmann et al., 2013). This effect, however, was overcome when later time points of cultivation were considered. Taken together, the primary location at the TSS and the major defect in SM production at earlier stages indicate a role for H3K14ac in transcriptional initiation. Furthermore, hyper-acetylation at H3K14 could be relevant for marking active genes and providing a docking side for regulatory proteins. The low correlation of gene expression and H3 acetylation might be explained by a greater spatial phasing rather than strong changes in the level of H3K14ac. However, at this stage also different specificity of the antibodies resulting in the shown acetylation profiles for both modifications cannot be excluded.

S. rapamycinicus silences fungal nitrogen metabolism

A substantial number of genes involved in primary and secondary nitrogen metabolism were strongly depleted for H3K9ac. This correlated with reduced expression of the respective genes measured by microarray and qRT-PCR analyses. Thus, upon contact with the bacterium *A. nidulans* silenced nitrogen uptake and degradation of various nitrogen sources, leading to nitrogen starvation. In *A. nidulans* nitrogen starvation leads to AreA-mediated histone H3 acetylation at nitrate gene promoters (Berger et al., 2008).

Under low nitrogen conditions like nitrogen starvation or low availability of primary nitrogen sources, such as glutamine and ammonium, the intracellular level of glutamine drops (Tudzynski, 2014). This was in fact observed for the intracellular concentration of amino acids in *A. nidulans*. These findings support the hypothesis that in presence of *S. rapamycinicus* but not of non-inducing streptomycetes (*e.g. S. lividans*) the fungus is in a physiological state of nitrogen starvation (Fig. 10). This finding further underlines the specificity of the interaction of *S. rapamycinicus* with *A. nidulans*. Interestingly, nitrogen availability is a trigger for the activation of a multitude of SM gene clusters including the *ors* gene cluster (Feng and Leonard, 1998, Scherlach et al., 2011, Studt et al., 2012, Niehaus et al., 2014). Nitrogen starvation also activates the expression of the anthrone (*mdp*) gene cluster (Scherlach et al., 2011), which we also observed in our data. However, induction of orsellinic acid production by nitrogen deficiency took about 60 h, whereas co-cultivation already triggered expression of the cluster after 3 h. Therefore, it is unlikely that the bacteria-triggered activation of the cluster is exclusively achieved by restricting nitrogen availability for the fungus. Furthermore, shortage of nitrogen leads to de-repression of genes involved in the usage of secondary nitrogen sources, which was not obvious from our data. In *S. cerevisiae*, it was shown that a shift from growth under nutrient sufficiency to nitrogen

starvation induced degradation of mitochondria (Eiyama et al., 2013). Interestingly, upon contact with the bacterium decreased acetylation and transcription of genes with mitochondrial function were also detected. This was further supported by a lower mitochondrial metabolic activity in the fungal cells during co-cultivation. Responsible for the degradation of mitochondria in yeast is a tightly controlled process called mitophagy which is independent of canonical autophagy (Kanki and Klionsky, 2008). Since *S. rapamycinicus* produces rapamycin, which is known to induce autophagy in filamentous fungi (Dementhon et al., 2003, Kim et al., 2011), we also tested a *Streptomyces iranensis* mutant deficient in rapamycin biosynthesis. Because this mutant was still able to induce the *ors* gene cluster, rapamycin does not play a role in induction (data not shown).

BasR is a central regulatory node for integrating bacterial signals leading to regulation of SM gene clusters

Another consequence of nitrogen starvation is the reduced availability of amino acids in the cell. Consequently, as shown here, the amino acid biosynthetic pathways represented a major group of de-regulated genes at both the acetylation level and the expression level. Amino acid biosynthesis in fungi is regulated by the cross-pathway control system (*cpc*) (Tudzynski, 2014). Since deletion of the central cross-pathway control gene *cpcA* in *A. nidulans* did not affect the induction of the *ors* gene cluster (Fig. S5), but on the other hand the artificial inducer of the cross-pathway control system 3-AT (Sachs, 1996) induced the production of orsellinic and lecanoric acid already after 24 h, it was reasonable to assume that cross-pathway control somehow plays a role. 3-AT is a structural analogue of histidine triggering histidine starvation in the fungal cell and thereby the cross-pathway control (Sachs, 1996). In *S. cerevisiae*, other regulators were also shown to induce the histidine

biosynthesis gene promoter *HIS7* upon purine starvation. This is achieved by cooperation of the *S. cerevisiae* Gcn5 with the heterodimeric transcription factor Bas1/Bas2p (Valerius et al., 2003, Daignan-Fornier and Fink, 1992). In contrast to the *S. cerevisiae* Bas1 protein (811 amino acids, Zhang et al., 1997) the *A. nidulans* orthologue identified here only consists of 305 amino acids with an N-terminal Myb-like domain. The C-terminal activation and regulatory (BIRD) domain of Bas1, which was described to mediate the Bas1p-Bas2p interaction (Pinson et al., 2000), is missing in the *A. nidulans* BasR. As shown here, *basR* was highly up-regulated in the microarray data which coincided with increased H3K9 acetylation of the gene promoter.

basR deletion and overexpression clearly demonstrated the function of this transcription factor in activating the *ors* gene cluster in dependence of *S. rapamycinicus*. Interestingly, the *basR* gene could not be found in all fungal genomes analyzed here, but for example in *A. sydowii* where also an *ors* gene cluster was found by bioinformatics analysis. As in *A. nidulans*, overexpression of the *A. sydowii basR* gene led to the activation of the silent *ors* gene cluster. Based on this finding we predicted that *S. rapamycinicus* also induces the *ors* gene cluster in *A. sydowii* which indeed was the case.

Genome-wide ChIP-seq analysis also indicated that the interaction of *S. rapamycinicus* with *A. nidulans* influenced other SM gene clusters, *e.g.*, it led to repression of the formation of emericellamides. Most interestingly, also for this repression, BasR was required, indicating that overexpression of *basR* phenocopies the regulation by *S. rapamycinicus*. Our data suggest that BasR represents a regulator required for transduction of signals perceived from the bacterium leading to the regulation of SM gene clusters (Fig. 10).

Materials and Methods

Microorganisms, media and cultivation. Microorganisms are listed in Table 2. *A. nidulans* strains were cultivated in *Aspergillus* minimal medium (AMM) at 37 °C and 200 rpm (Brakhage and Van den Brulle, 1995). AMM was supplemented according to the requirements of the strains as follows: arginine (871 µg/mL), *p*-aminobenzoic acid (3 µg/mL) and pyridoxine HCl (5 µg/mL). Pre-cultures were inoculated with 4×10^8 spores per mL. 10 µg/mL doxycycline was used to induce the tet^{On} inducible system. For the measurement of orsellinic acid, mycelia of overnight cultures (~16 h) in AMM were transferred to fresh medium and inoculated with *S. rapamycinicus*, as described by Schroeckh et al. (2009). RNA extraction for expression analysis during co-cultivation was performed after 3 h of cultivation. For the expression analysis of the *basR* overexpression mutant samples for RNA extraction were taken after 6 h of cultivation; samples for HPLC analysis were taken after 24 h. *A. sydowii* was cultivated at 28 °C and 200 rpm in malt medium (Scherlach et al., 2010). For the induction of the *ors* cluster, 48-hour old precultures grown at 28 °C in malt medium were first transferred to fresh AMM and inoculated with *S. rapamycinicus* or doxycycline. Doxycycline was added twice over the course of 48 hours, adding up to a final concentration of 20 µg/mL. The cultures were allowed to grow at 28 °C; samples were taken for LC-MS analysis after 96 hours for *A. sydowii* co-cultivation and after 48 hours for the *basR* overexpression mutant.

For MALDI-MS Imaging analysis conductive ITO slides (Bruker Daltonics, Bremen, Germany) were coated with 3 mL 0.5% (w/v) AMM agar and incubated at room temperature for 30 minutes (Araújo et al., 2017, Aiyar et al., 2017). Equal conditions were ensured by supplementing all slides with arginine regardless of the fungal genotype. 20 µg/mL doxycycline was used to induce the tet^{On} inducible system. *S. rapamycinicus* was applied by

filling 5 mL of a preculture in a tube for 10 minutes and point inoculation of 15 µl of the settled *S. rapamycinicus* mycelium on the agar. *A. nidulans* and its respective mutants were applied by point inoculation of 500 spores. For co-cultivation experiments, the fungus and the streptomycete were inoculated 1 cm apart from each other. The slides were incubated at 37 °C in a petri dish for 4 days. After incubation, the fungal spores were removed with adhesive tape. The slides were dried by incubation in a hybridization oven at 37 °C for 48 hours.

qRT-PCR. Expression levels were quantified by qRT-PCR. Total RNA was purified with the Universal RNA Purification Kit (roboklon, Berlin, Germany) according to the manufacturer's instructions including DNase I treatment. Reverse transcription of 5 µg RNA was performed with RevertAid Reverse Transcriptase (Thermo Fisher Scientific, Darmstadt, Germany) for 3 h at 46 °C. cDNA was amplified on an Applied Biosystems StepOnePlus Real-Time PCR system (Foster City, USA). Quantitative RT-PCR of 3 ng/µl cDNA samples was performed with MyTaq HS mix 2x (Bioline, Luckenwalde, Germany) and EvaGreen (Biotium, Fremont, California, USA) using primers for the respective target genes (Table S2). The PCR parameters included an initial DNA denaturation step at 95 °C for 2 min, followed by 45 cycles with DNA denaturation at 95 °C for 5 s and primer annealing and extension at 62 °C for 15 s. The *A. nidulans* ß-actin gene (*AN6542*) was used as an internal standard for calculation of expression levels as previously described (Schroeckh et al., 2009).

Preparation of chromosomal DNA and Southern blot analysis. *A. nidulans* genomic DNA was isolated as previously described (Schroeckh et al., 2009). Southern blotting was done using a digoxigenin-11-dUTP-labelled (Jena Bioscience, Jena, Germany) probe, as previously described (Schroeckh et al., 2009). Primers for amplification of probes are listed in Table S2.

ChIP coupled to qRT-PCR analysis. Cultures were essentially grown as described above and after 3 h the DNA was cross-linked to the proteins for 15 min with 1 % (v/v) formaldehyde at room temperature. To stop the reaction glycine was added to a final concentration of 125 mM for 5 min at 37 °C and the sample was subsequently frozen in liquid nitrogen. Powdered mycelium was dissolved in 1 ml of sonication buffer (50 mM HEPES-KOH pH 7.5, 140 mM NaCl, 1 mM EDTA, 1 % (v/v) Triton X-100, 0.1 % (w/v) Na-deoxycholate, 1 x Fungal protease inhibitor mix (Promega, Madison, Wisconsin, USA)) and 330 µl aliquots were then subjected to sonication for 30 min with cycles of 2 min maximum intensity followed by a 1 min pause. Sheared chromatin was separated from cell wall debris and incubated with 40 µl of a protein A slurry for 30 min at 4 °C on a rotary shaker. A purified 1:10 dilution of the supernatant was then incubated overnight at 4 °C with 3 µl of antibody directed against the desired target. Antibodies were precipitated with 40 µl of Dynabeads (Invitrogen, Carlsbad, California, USA) which were incubated with the sample for 40 min at 4 °C on a rotary shaker. Samples were washed 3 times with low salt buffer (150 mM NaCl, 0.2 % (w/v) SDS, 0.5 % (v/v) Triton X-100, 2 mM EDTA, 20 mM Tris-HCl pH 8) followed by one time washing with high salt buffer (500 mM NaCl, 0.2 % (w/v) SDS, 0.5 % (v/v) Triton X-100, 2 mM EDTA, 20 mM Tris pH 8). Washed beads were dissolved in 125 µl TES buffer and reverse cross-linked by co-incubation with 2 µl of 0.5 M EDTA, 4 µl of 1 M Tris-HCl pH 6.5 and 2 µl of 1 mg/mL proteinase K for 1 h at 45 °C. Subsequent DNA purification was conducted with a PCR purification kit and samples were eluted in 100 µl of 1:10 diluted elution buffer. Concentration of DNA of genes of interest was quantified using qRT-PCR essentially as described above. Antibodies used are the following: mouse monoclonal ANTIFLAG M2 (Sigma-Aldrich, F3165-5MG, Taufkirchen, Germany), rabbit polyclonal anti-histone H3 (Abcam 1791, Cambridge, UK), rabbit polyclonal histone H3K9ac (Active Motif, Catalog No:

524 39161, La Hulpe, Belgium) and rabbit polyclonal anti-acetyl-histone H3 (Lys14) (Merck
525 Millipore, Darmstadt, Germany).

526 **Extraction of compounds from *A. nidulans* and HPLC analysis.** Culture broth containing
527 fungal mycelium and bacteria was homogenized utilizing an ULTRA-TURRAX (IKA-Werke,
528 Staufen, Germany). Homogenized cultures were extracted twice with 100 mL ethyl acetate,
529 dried with sodium sulfate and concentrated under reduced pressure. For HPLC analysis, the
530 dried extracts were dissolved in 1.5 mL of methanol. Analytical HPLC was performed using a
531 Shimadzu LC-10Avp series HPLC system composed of an autosampler, high pressure pumps,
532 column oven and PDA. HPLC conditions: C18 column (Eurospher 100-5 250 x 4.6 mm) and
533 gradient elution (MeCN/0.1 % (v/v) TFA (H_2O) 0.5/99.5 in 30 min to MeCN/0.1 % (v/v) TFA
534 100/0, MeCN 100 % (v/v) for 10 min), flow rate 1 mL min^{-1}; injection volume: 50 µL.
535 Identification of metabolites was achieved by comparison with an authentic reference.
536 Samples were quantified *via* integration of the peak area using Shimadzu Class-VP software
537 (version 6.14 SP1).

538 **Extraction of compounds from *A. sydowii* and HPLC analysis.** Culture broth containing the
539 fungal mycelium was homogenized using a T 25 ULTRA-TURRAX (IKA-Werke, Staufen,
540 Germany). Homogenized cultures were extracted twice with equal volume of ethyl acetate,
541 dehydrated with anhydrous sodium sulfate, filtered and reduced to dryness with a rotary
542 evaporator (Laborota 4000 efficient; Heidolph Instruments, Schwabach, Germany). The
543 crude extracts were reconstituted in 1 mL methanol and filtered through a 0.2-µm-pore-size
544 polytetrafluoroethylene filter (Carl Roth, Karlsruhe, Germany). The samples were loaded
545 onto an ultrahigh-performance liquid chromatography (LC)–mass spectrometry system
546 consisting of an UltiMate 3000 binary rapid-separation liquid chromatograph with
547 photodiode array detector (Thermo Fisher Scientific, Dreieich, Germany) and an LTQ XL

548 linear ion trap mass spectrometer (Thermo Fisher Scientific, Dreieich, Germany) equipped
549 with an electrospray ion source. The extracts (injection volume, 10 µl) were analyzed on a
550 150- by 4.6-mm Accucore reversed-phase (RP)-mass spectrometry column with a particle
551 size of 2.6 µm (Thermo Fisher Scientific, Dreieich, Germany) at a flow rate of 1 mL/min, with
552 the following gradient over 21 minutes: initial 0.1% (vol/vol) HCOOH-MeCN/0.1% (vol/vol)
553 HCOOH-H_2O 0/100, which was increased to 80/20 in 15 min and then to 100/0 in 2 min, held
554 at 100/0 for 2 min, and reversed to 0/100 in 2 minutes. Identification of metabolites was
555 achieved by comparison with an authentic reference.

556 **Measurement of amino acids.** Amino acids were extracted from 10 mg samples with 1 mL of
557 methanol and the resulting extract was diluted in a ratio of 1:10 (v:v) in water containing the
558 ^{13}C, ^{15}N labeled amino acid mix (Isotec, Miamisburg, Ohio, USA). Amino acids in the diluted
559 extracts were directly analyzed by LC-MS/MS as described with the modification that an
560 API5000 mass spectrometer (Applied Biosystems, Foster City, California, USA) was used
561 (Docimo et al., 2012).

562 **Resazurin assay.** Metabolic activity was measured by the resazurin reduction to the
563 fluorescent dye resorufin. 10^4 conidia of *A. nidulans* in 100 µl AMM were pipetted in each
564 well of a black 96 well plate. Incubation of the plate was performed for 16 h at 37 °C. The
565 pre-grown fungal mycelium was further incubated in monoculture or together with 10 µl of
566 an *S. rapamycinicus* culture. Cultures were further supplemented with 100 µl of AMM
567 containing resazurin in a final concentration of 0.02 mg/mL. Fluorescence was measured
568 (absorption wavelength 560 nm, emission wavelength 590 nm) every 30 minutes for 24 h at
569 37 °C in a Tecan Fluorometer (Infinite M200 PRO, Männedorf, Switzerland). To assure
570 physical contact of fungal and bacterial cells the plate was shaken for 30 seconds before
571 measurement. The medium control consisted of 100 µl AMM and 100 µl resazurin solution.

572 For all conditions, measurements were carried out in triplicates for each of the two
573 biological replicates. Significance of values was calculated using 2-way ANOVA Test with
574 GraphPad Prism 5 (GraphPad Software Inc., La Jolla, California, USA).

575 **ChIP-seq pre-processing.** The *A. nidulans* FGSC A4 genome and annotation (version s10-
576 m03-r28) were obtained from the data warehouse AspGD. The *S. rapamycinicus* NRRL 5491
577 genome was obtained from NCBI (GI 521353217). *A. nidulans* and *S. rapamycinicus* genomes
578 were concatenated to a fused genome to serve as the reference genome for subsequent
579 mapping. Quality control was carried out and raw ChIP-seq reads were obtained by using
580 FastQC v0.11.4. Trimming and filtering were achieved by applying Trim Galore utilizing
581 Illumina universal adapter and phred+33 encoding. Reads were not de-duplicated since the
582 duplication rate was < 15% for most libraries. Bowtie2 (version 2.2.4) using default
583 parameters was employed to map reads to the fused genome. Quantification of reads was
584 carried out using the Bioconductor 'GenomicAlignments' package forming the basis for three
585 subsequent approaches. Firstly, a genome-wide equi-spaced binning across the genome with
586 different resolutions (50k and 2k bp bins) counting reads overlapping each bin was applied.
587 Library normalization on bin counts was performed by only considering reads mapping to
588 the *A. nidulans* genome. Secondly, reads overlapping genes were counted, using the AspGD
589 annotation. They formed the basis for the subsequent DCS analysis (see below). Thirdly,
590 average profile plots to assess relative histone distributions around TSS and TTS were
591 generated using the bioconductor package regioneR (Gel et al., 2016).

592 **Differential chromatin state analysis (DCS analysis).** To identify genes exhibiting differences
593 in their chromatin state, we employed the bioconductor package edgeR (Robinson and
594 Oshlack, 2010) originally developed for RNA-seq differential expression analysis but the
595 assumptions equally hold for ChIP-seq data, *i.e.*, negative binomial distribution of reads.

Importantly, library normalization was achieved with the TMM (trimmed mean of M values, Robinson and Oshlack, 2010) method only based on *A. nidulans* gene counts for calculating the effective library sizes, not taking into account reads mapping to *S. rapamycinicus* which would otherwise artificially influence the effective library size. Comparisons were made between libraries for all ChIP targets separately obtained from monocultures of *A. nidulans* and co-cultures with *S. rapamycinicus.* These targets were H3, H3K9ac and H3K14ac. Results including normalized read counts (RPKM) statistics and log fold changes (LFCs) are reported in Table S1. Normalized counts and LFCs were also further used for comparisons with the corresponding microarray-based gene expression and LFCs.

MACS analysis. Candidate peaks were identified using two methods: a differential binding analysis (EdgeR) and a peak-calling approach (MACS, version 2.0.1) (Zhang et al., 2008). The peak caller performed several pairwise comparisons between samples with the same antibody and different conditions in order to retrieve the differentially bound peaks for that particular comparison. The program kept the track of different replicates, the signal was reported per million reads and produced a BED format track of the enriched regions, the other parameters were used with default values. The BED files were subsequently converted to Big Wig format for visualization through the tool Integrative Genomics Viewer (Thorvaldsdóttir et al., 2013).

MALDI-MS imaging analysis and data processing. Conductive ITO slides inoculated with *A. nidulans* and *S. rapamycinicus* were dried overnight at 37 °C in a hybridization oven and sprayed with a saturated solution (20 mg/mL) of universal MALDI matrix (1:1 mixture of 1:1 mixture of 2,5-dihydroxybenzoic acid and α-cyano-4-hydroxy-cinnamic acid; Sigma Aldrich, Taufkirchen, Germany) in acetonitrile/methanol/water (70:25:5, v:v:v), using the automatic system ImagePrep device 2.0 (Bruker Daltonics, Bremen, Germany) in 60 consecutive cycles

(the sample was rotated 180 ° after 30 cycles) of 52 seconds (2 s spraying, 10 s incubation time, and 40 s of active drying) as recommended in Hoffmann and Dorrestein (2015). The sample was analyzed using an UltrafleXtreme MALDI TOF/TOF (Bruker Daltonics, Bremen, Germany), which was operated in positive reflector mode using flexControl 3.0. The analysis was performed in the 100-3000 Da range, with 30 % laser intensity (laser type 4), accumulating 1000 shots by tanking 50 random shots at every raster position. Raster width was set at 200 µm. Calibration of the acquisition method was performed externally using Peptide Calibration Standard II (Bruker Daltonics, Bremen, Germany) containing Bradykinin1-7, Angiotensin II, Angiotensin I, Substance P, Bombesin, ACTH clip1-17, ACTH clip18-39, Somatostatin28. Spectra were processed with baseline subtraction in flexAnalysis 3.3 (Bruker Daltonics, Bremen, Germany) and corrected internally using the peaks of HCCA ($[M+H]^+$ *m/z* 190.0499 and $[2M+H]^+$ *m/z* 379.0925). Processed spectra were uploaded in flexImaging 3.0 (Bruker Daltonics, Bremen, Germany) for visualization and SCiLS Lab 2015b (Bruker Daltonics, Bremen, Germany) for analysis and representation. Chemical image were obtained using Median normalization and weak denoising. The experiment was replicated three times, the 2^{nd} and 3^{rd} replicates were measured at 250 µm raster width.

Generation of *A. nidulans* deletion strains. The transformation cassettes for the *basR* and *cpcA* deletion strains were constructed as previously described (Szewczyk et al., 2007). Approximately ~1000-bp sequences homologous to the regions upstream and downstream of *basR* and *cpcA* were amplified and fused to the *argB* deletion cassette (Schroeckh et al., 2009). Transformation of *A. nidulans* was carried out as described before (Ballance and Turner, 1985).

Generation of an inducible *A. nidulans basR* overexpressing mutant strain. For controlled overexpression of the putative Myb-like transcription factor gene *basR*, the tetracycline-

644 controlled transcriptional activation system (*tet*^{On}) system was used (Helmschrott et al.,
645 2013). The corresponding gene sequences together with their ~1000-bp flanking regions
646 were amplified from *A. nidulans* genomic DNA using the Phusion Hot Start Flex DNA
647 Polymerase (New England Biolabs, Frankfurt, Germany) according to the manufacturer's
648 instructions. The *A. nidulans pabaA* gene, complementing the *p*-aminobenzoic acid
649 auxotrophy of the recipient strain, was used as a selectable marker. The *tet*^{On}-system was
650 amplified from the plasmid pSK562. All DNA fragments were assembled by using NEBuilder
651 HiFi DNA Assembly Master Mix (New England Biolabs, Frankfurt, Germany) according to the
652 manufacturer's instructions. For this purpose, an additional *Dra*III restriction site was
653 inserted in pJET1 vector (Thermo Fisher Scientific, Darmstadt, Germany). The assembled
654 12.3-kb plasmid was restricted with *Dra*III to obtain a linear DNA fragment, which was used
655 to complement the generated *A. nidulans* Δ*basR* mutant strain.

656 **Generation of an inducible *A. sydowii basR* overexpressing mutant strain.** For the
657 overexpression of the putative Myb-like transcription factor gene *basR* in *A. sydowii*, the
658 tetracycline-controlled transcriptional activation system (*tet*^{On}) system was used
659 (Helmschrott et al., 2013). An expression vector was constructed by amplifying the *A.*
660 *sydowii basR* gene from *A. sydowii* genomic DNA using the Phusion Flash High-Fidelity PCR
661 Master Mix (Thermo Fisher Scientific, Dreieich, Germany) according to the manufacturer's
662 instructions. The *A. oryzae hph* cassette was used as a selectable marker. The *tet*^{On}-system
663 was amplified from the plasmid pSK562. All DNA fragments were assembled by using
664 NEBuilder HiFi DNA Assembly Master Mix (New England Biolabs, Frankfurt, Germany)
665 according to the manufacturer's instructions. The assembled 9.1 kb plasmid was used for
666 transformation of *A. sydowii* wild type. 200 µg/mL hygromycin was used as selection agent in
667 all following media (Invivogen, Toulouse, France).

Phylogenetic analysis. The amino acid sequences for the two Myb-like transcription factors from *A. nidulans* (*AN7174* (*basR*) and *AN8377*) and Bas1 from *S. cerevisiae* were used for a Blast search in the UniProtKB database (http://www.uniprot.org). For each sequence, the first 50 hits were retrieved. All hits were grouped together, and redundant and partial sequences removed. The obtained 54 hits were firstly aligned using MUSCLE (Edgar, 2004), and then the phylogenetic tree was obtained using the Maximum Likelihood method contained in the MEGA6 software facilities (Tamura et al., 2013).

Accession

ChIP-seq data were deposited in the ArrayExpress database at EMBL-EBI (www.ebi.ac.uk/arrayexpress) under accession number E-MTAB-5819. For access use: Username: Reviewer_E-MTAB-5819; Password: XNLK26QT. Code for data processing and analysis can be obtained from https://github.com/seb-mueller/ChIP-Seq_Anidulans.

Acknowledgements

We thank Christina Täumer and Karin Burmeister for excellent technical assistance and Sven Krappmann (Friedrich-Alexander University, Erlangen-Nürnberg, Germany) for kindly providing plasmid pSK562. Financial support by the Deutsche Forschungsgemeinschaft (DFG)-funded excellence graduate school *Jena School for Microbial Communication* (JSMC), the *International Leibniz Research School for Microbial and Biomolecular Interactions* (ILRS) as part of the JSMC, the DFG-funded *Collaborative Research Center 1127 ChemBioSys* (projects B01, B02 and INF) and the ERC for a Marie Skłodowska-Curie Individual Fellowship (IF-EF; Project reference 700036) to María García-Altares are gratefully acknowledged.

691 **Tables**

692 **Table 1.** List of selected genes with differentially acetylated H3K9 residue and with log-fold

693 change (LFC) in microarray data.

			ChIP-seq	Microarray
Name	**Annotation**	**Description**	**LFC H3K9ac**	**LFC**
Nitrogen metabolism				
crnA	AN1008	Nitrate transporter with 12 predicted *trans*-membrane domains	-1.30	-1.00
niaD	AN1006	Nitrate reductase (NADPH)	-1.78	-1.03
niiA	AN1007	Nitrite reductase	-1.92	-1.10
tamA	AN2944	Transcriptional co-activator of the major nitrogen regulatory protein AreA	-0.80	-1.27
gltA	AN5134	Glutamate synthase, NAD^+-dependent (GOGAT)	-0.86	-1.37
gdhA	AN4376	NADP-linked glutamate dehydrogenase	-1.14	1.04
ntpA	AN5696	Nitric oxide-induced nitrosothionein involved in NO detoxification	-1.16	-1.15
meaA	AN7463	Major ammonium transporter	-1.22	-1.12
ureD	AN0232	Nickel-binding protein involved in utilization of urea as a nitrogen source	-1.44	-1.94
prnD	AN1731	Proline dehydrogenase with a predicted role in proline metabolism	-1.36	1.01
prnB	AN1732	Proline transporter	-1.39	-1.39
Amino acid metabolism				
ugeA	AN4727	UDP-glucose 4-epimerase, involved in galactose metabolism	-0.82	-1.54
qutB	AN1137	Quinate 5-dehydrogenase with a role in aromatic amino acid biosynthesis	-0.90	1.39
	AN9506	Protein with predicted amino acid *trans*-membrane transporter activity, role in amino acid *trans*-membrane transport and membrane localization	-0.98	-1.60

	AN1923	Putative alanine transaminase with a predicted role in alanine and aspartate metabolism	-1.02	1.13
	AN5731	Putative chorismate synthase with a predicted role in aromatic amino acid biosynthesis	-1.04	1.02
	AN6255	Putative cytochrome c oxidase subunit with a predicted role in energy metabolism	-1.08	1.28
	AN8118	Putative cytochrome c oxidase subunit with a predicted role in energy metabolism	-1.08	1.26
	AN1150	Putative transaminase with a predicted role in arginine metabolism	-0.62	1.07
	AN1733	Putative delta-1-pyrroline-5-carboxylate dehydrogenase with a predicted role in glutamate and glutamine metabolism	-0.79	-1.35
	AN2129	Subunit 5 of the COP9 signalosome (CSN) responsible for cleaving the ubiquitin-like protein Nedd8 from cullin-RING E3 ubiquitin ligases	-0.50	-2.23
	AN3347	Putative amino acid transporter	-0.64	Not detectable
	AN8647	High-affinity nitrite transporter	-0.59	-3.90
	AN0399	High-affinity nitrate transporter	-0.59	1.16
	AN0418	Putative high-affinity urea/H^+ symporter	-0.58	1.06
	AN7379	Orthologue(s) have role in negative regulation of transcription from RNA polymerase II promoter, regulation of nitrogen utilization and nucleus localization	0.51	1.26
cpcA	AN3675	Transcription factor of the Gcn4p c-Jun-like transcriptional activator family	1.02	2.88
jlbA	AN1812	bZIP transcription factor	1.3	1.03
Calcium signaling				
	AN3585	Transcript induced in response to calcium dichloride in a CrzA-dependent manner	1.42	13.22
pmcB	AN4920	Calcium-transporting	1.42	3.16

		mitochondrial ATPase involved in calcium homeostasis		
	AN3998	Transcript induced in response to calcium dichloride in a CrzA-dependent manner	1.26	2.01
	AN3420	Transcript induced in response to calcium dichloride in a CrzA-dependent manner	1.05	2.24
	AN4418	Transcript induced in response to calcium dichloride in a CrzA-dependent manner	1.03	-1.02
	AN2427	Transcript induced in response to calcium dichloride in a CrzA-dependent manner	1.00	2.11
	AN0419	Transcript induced in response to calcium dichloride in a CrzA-dependent manner	0.88	-1.99
	AN3751	Transcript induced in response to calcium dichloride in a CrzA-dependent manner	0.86	11.83
	AN5372	Transcript induced in response to calcium dichloride in a CrzA-dependent manner	0.82	-1.79
	AN5993	Has domain(s) with predicted calcium binding activity	0.76	271.00
	AN5341	Orthologue(s) have calcium binding activity	0.74	-1.26
	AN2826	Transcript induced in response to calcium dichloride in a CrzA-dependent manner	0.73	4.34
	AN1950	Orthologue(s) have FAD *trans*-membrane transporter activity, calcium channel activity	0.72	-1.20
	AN5302	Transcript induced in response to calcium dichloride in a CrzA-dependent manner	0.64	2.21
mid1	AN8842	Stretch-activated calcium channel	0.63	-1.00
pmrA	AN7464	Calcium-transporting ATPase with a predicted role in energy metabolism	-0.74	-1.60
	AN8774	Transcript induced in response to calcium dichloride in a CrzA-dependent manner	0.55	2.40
Development				
	AN4674	Orthologue(s) have role in asexual sporulation resulting in	1.14	1.21

		formation of a cellular spore, cellular response to drug and cell septum, cell surface localization		
mstC	AN6669	High-affinity glucose transporter active in germinating conidia	0.92	2.79
	AN0928	Orthologue(s) have role in conidiophore development	0.90	1.00
	AN5619	Orthologue(s) have metallopeptidase activity, role in ascospore wall assembly and ascospore wall, endoplasmic reticulum membrane localization	0.88	1.29
fbx15	AN2505	F-box protein	0.88	2.38
	AN2856	Orthologue(s) have 3'-5' exonuclease activity, role in ascospore formation, conversion of ds siRNA to ss siRNA involved in RNA interference, fruiting body development, pre-miRNA processing and perinuclear region of cytoplasm localization	0.80	2.83
	AN3689	Orthologue(s) have role in ascospore formation and cytosol, nucleus localization	0.69	1.73
esdC	AN9121	Protein with a glycogen binding domain involved in sexual development	0.68	1.69
	AN6898	Orthologue(s) have role in asexual sporulation resulting in formation of a cellular spore, intralumenal vesicle formation and protein retention in Golgi apparatus, more	0.65	-1.21
	AN1131	Putative cytosolic Cu/Zn superoxide dismutase	0.63	1.13
	AN3813	Orthologue(s) have copper uptake *trans*-membrane transporter activity and role in aerobic respiration, copper ion import, hyphal growth, spore germination, sporocarp development involved in sexual reproduction	0.58	-3.48
MAT1	AN2755	Alpha-domain mating-type	0.52	1.22

		protein		
fcyB	AN10767	Purine-cytosine transporter	-0.58	
tmpA	AN0055	*Trans*-membrane protein involved in regulation of conidium development	-0.58	-8.61
fluG	AN4819	Cytoplasmic protein involved in regulation of conidiation and sterigmatocystin production	-0.66	1.35
cffA	AN5844	Orthologue of *Neurospora crassa conF*, light-induced transcript expressed during conidiation in *N. crassa*	-0.71	2.66
gsk3	AN6508	Protein kinase	-0.80	-1.53
rasA	AN0182	Small monomeric GTPase of the Ras superfamily involved in regulation of development	-0.81	-1.38
***ors* gene cluser**				
orsD	AN7913	Protein of unknown function	2.64	23.06
orsB	AN7911	Putative amidohydrolase	2.32	158.75
orsC	AN7912	Putative tyrosinase	2.28	21.19
orsE	AN7914	Putative alcohol dehydrogenase	1.58	57.62
orsA	AN7909	Polyketide synthase	1.57	120.33
***atn* gene cluster**				
	AN7877	RTA-like protein	0.87	1.37
	AN7875	Protein of unknown function	1.09	4.23
	AN7883	Protein of unknown function	1.04	119.22
***dba* gene custer**				
cipB	AN7895	Putative oxidoreductase	0.89	14.48
dbaB	AN7897	FAD-binding monooxygenase with a role in secondary metabolism	0.80	997.83
dbaA	AN7896	$Zn(II)_2Cys_6$ transcription factor with a role in secondary metabolite biosynthesis	0.77	80.40
Cichorin gene cluster				
	AN6440	Orthologue of *Aspergillus versicolor* Aspve1_0168042, *Aspergillus sydowii* Aspsy1_0031884 and *Aspergillus carbonarius* ITEM 5010 : Acar5010_000187	0.76	14.45
	AN6441	Protein of unknown function	0.77	6.97
cicE	AN6447	Predicted O-methyltransferase	0.62	1.13
	AN6437	Orthologue of *Aspergillus versicolor* Aspve1_0052718 and *Aspergillus sydowii*	1.04	-1.31

		Aspsy1_0031878		
***stc* gene cluster**				
stcO	AN7811	Sterigmatocystin biosynthesis protein with a role in sterigmatocystin/aflatoxin biosynthesis	0.58	-1.93
stcI	AN7816	Sterigmatocystin biosynthesis lipase/esterase with a role in sterigmatocystin/aflatoxin biosynthesis	0.59	1.21
stcE	AN7821	Norsolorinic acid reductase with a role in sterigmatocystin/aflatoxin biosynthesis	0.48	1.47
***mdp* gene cluster**				
mdpD	AN0147	Flavin-containing monooxygenase	0.57	1.14
***eas* gene cluster**				
easD	AN2549	Acyl-CoA ligase; required for emericellamide biosynthesis; emericellamide (*eas*) biosynthetic gene cluster member	-1.07	-20.90
easC	AN2548	Acyltransferase	-0.58	-14.23

694

695 **Table 2.** List of strains used in this study.

Strain	**Genotype**	**Reference**
Aspergillus nidulans		
A1153	*yA1*, *pabaA1*; *argB2*; *pyroA4*, *nkuA::bar*	Nayak et al., 2006
A1153*gcnE-3xflag*	*yA1, pabaA1; gcnE::gcnEp-gcnE-3x-flag-pabaA1; pyroA4, nkuA::bar*	Nützmann et al., 2011
A1153Δ*cpcA*	*yA1, pabaA1; cpcA::argB2; pyroA4,*	This study

Strain	**Genotype**	**Reference**
	nkuA::bar	
A1153Δ*basR*	*yA1, pabaA1; basR::argB2; pyroA4, nkuA::bar*	This study
A1153*tet*^{On}*-basR*	*yA1, pabaA1; argB2::pabaA1-tet*^{On}*-basR; pyroA4, nkuA::bar*	This study
Aspergillus sydowii		
CBS 593.65		Westerdijk Fungal Bio Diversity Institute
tet^{On}*-basR*	Ectopic integration of pUC18 *tet*^{ON}*-basR-hph*	This study
***Streptomyces rapamycinicus* ATCC 29253**		Kumar and Goodfellow, 2008
***Streptomyces lividans* TK24**		Kieser et al., 2000

696

697

698

699

700

701

Legends to the Figures

Figure 1. Genome-wide coverage plot of the merged fungal-bacterial genome with indication of H3(Cterm) and acetylated H3 (K9 and K14). For each condition, ChIP-seq analyses of three independent samples were performed. (**A**) Genome-wide analysis covering all chromosomes. Data for each chromosome, *i.e.*, I to VIII are shown. X axis corresponds to genome coordinates of the fused genome in Mb. Y axis corresponds to the number of reads mapping within equally sized windows (bins) which segment the fused genome at a resolution of 50 kb for each library separately (see methods for details). The reads count value is plotted at the midpoint of each bin which were then connected by lines. Gene density is reported likewise by counting the number of genes for each bin instead of reads. Background values derive from *S. rapamycinicus* and *A. nidulans* grown in monoculture. The red arrow indicates the location of the *ors* gene cluster. (**B**) Zoom into chromosome II. The red lines mark the *ors* gene cluster. Data of three replicates are shown, which show the same tendency. Overall intensity of background, H3K9ac, H3K14ac and H3(Cterm) compared between *A. nidulans* mono culture (grey) and co-culture (blue) as well as the average genome density (black). (**C**) IGB screenshot of the *ors* gene cluster shown at the bottom of the figure labeled with black arrows. Blank gene arrows indicate genes not belonging to the *ors* gene cluster. Data obtained from monocultures of the fungus are depicted in blue, from co-cultivation in green and background data in grey.

Figure 2. Normalized read counts derived from differential chromatin state (DCS) analysis obtained for the *ors* genes based on H3, H3K14ac and H3K9ac ChIP-seq. Data were

generated for the area 500 bp down- and 1000 bp upstream from the TSS. Depicted bars are calculated from 3 data points.

Figure 3. Read count frequencies for (A) TSS and (B) TTS. Lines correspond to the relative enrichment of ChIP signal strength relative to the TSS/TTS averaged across all genes. ChIP-seq read count serves as a surrogate for signal strength (see methods for further details). Compared were the enrichment of histone H3 (black), H3K9ac (blue), H3K14ac (green) and the background control (grey) over an average of all TSS and TTS. The enrichment curves for all biological replicates are given, indicated by multiple lines per enrichment target.

Figure 4. Relation between ChIP-seq and microarray data. The blue lines resemble the linear regression line based on the differentially expressed genes with an adjusted *p*-value of < 0.1 including the confidence interval shown in grey. (**A**) LFC of H3K14ac plotted against LFC of H3K9ac. Dots depicted in dark grey and green mark differentially expressed genes and *ors* cluster genes, respectively. (**B**) Pairwise comparison of log fold changes (LFCs) of H3, H3K14ac and H3K9ac data with microarray data obtained during co-cultivation of *A. nidulans* with *S. rapamycinicus*.

Figure 5. Normalized ChIP-seq read counts were used to quantify chromatin state for individual genes. Here, for H3, H3K14ac and H3K9ac libraries nitrogen metabolism genes were shown. Counts were obtained by counting reads mapping to the promoter area for each gene that is 500 bp down- and 1000 bp upstream from the TSS. Depicted bars are calculated from 3 data points.

Figure 6. Characterization of nitrogen metabolism genes and genes with mitochondrial function. (**A**) Categorization of genes with FungiFun2 differentially lower acetylated at H3K9.

Nitrogen metabolism genes and genes with mitochondrial function are shaded in blue and green, respectively. (**B**) Transcription analysis of randomly selected genes of primary and secondary nitrogen metabolism by qRT-PCR during co-cultivation. Relative mRNA levels were measured after 3 h and normalized to the β-actin gene expression. The transcription of *orsA* was used as a positive control. (**C**) Metabolic activity comparing fungal co-cultivation with monocultures of *A. nidulans* and *S. rapamycinicus*. Metabolic activity was determined using a resazurin assay. Data were normalised to medium. The black line shows the time points that are significantly different between *A. nidulans* and the co-cultivation of *A. nidulans* with *S. rapamycinicus*. *** $p < 0.001$

Figure 7. **Expression of cross-pathway control regulatory genes, amino acid concentrations and their effect on SM production.** (**A**) Transcription of *cpcA* and *jlbA* determined by qRT-PCR after 3h of co-cultivation. Relative mRNA levels were compared to β-actin gene expression. (**B**) HPLC-based detection of orsellinic acid (1) and lecanoric acid (2) in supernatants of *A. nidulans* cultures treated with 3-AT. (**C**) Intracellular amino acid concentration of *A. nidulans* in monoculture and co-culture with *S. rapamycinicus*. Co-cultivation with *S. lividans* and addition of *S. rapamycinicus* after 24 h of cultivation served as negative controls. Furthermore, before extraction of amino acids the fungus (post cultivation) was also supplemented with *S. rapamycinicus* to exclude a bias resulting from the bacterial amino acids. Threonine, histidine, phenylalanine, arginine, asparagine and glutamine displaying differential concentrations in co-culture with the fungus are highlighted in grey.

Figure 8. The Myb-like transcription factor BasR of *A. nidulans* is required for *S. rapamycinicus*-triggered regulation of SMs. (**A**) Relative transcript levels of *ors* cluster genes

orsA and *orsD* in Δ*basR* mutant strain and *tet*^{On}-*basR* overexpression strain. Transcript levels were measured by qRT-PCR normalized to β-actin transcript levels. (**B**) HPLC-based detection of orsellinic acid and lecanoric acid in wild-type strain, *basR* deletion mutant and *basR* overexpression strain. (**C**) Visualization of ions *m/z* 646.3 and *m/z* 662.3 $^{+}$/- 1 Da, potentially corresponding to $[M+Na]^+$ and $[M+K]^+$ of emericellamide E/F ($C_{32}H_{57}N_5O_7$; accurate mass 623.4258), by MALDI-MS imaging. Images corrected by median normalization and weak denoising.

Figure 9. Fungal orsellinic acid gene clusters and their activation by BasR and the bacterium *S. rapamycinicus.* (A) Alignment of the orsellinic acid gene clusters in the fungal species containing a *basR* homologue (*A. nidulans*, *A. sydowii*, *A. versicolor*), where *orsA* encodes the polyketide synthase, while *orsB-orsF* code for the tailoring enzymes. **(B)** LC-MS-based detection of orsellinic acid and lecanoric acid in the monoculture of the *A. sydowii* *basR* overexpression strain following induction with doxycycline (left) and during co-cultivation of *A. sydowii* and *S. rapamycinicus* (right). LC-MS profiles of the extracted ion chromatogram (EIC) are shown for *m/z* 167 $[M - H]^-$, which corresponds to orsellinic acid. Orsellinic acid (1) and lecanoric acid (2), detected *via* its fragmention ion orsellinic acid.

Figure 10. **Model of the *S. rapamycinicus* – *A. nidulans* interaction.** Co-cultivation leads to nitrogen starvation and to reduced amino acid availability in the fungal cell. The lysine-acetyltransferase GcnE specifically acetylates (ac) lysine (K) 9 and 14 of histone H3 at the *ors* gene cluster and presumably at the *basR* gene promoter. As a consequence, *basR* is expressed. The deduced transcription factor BasR activates the ors gene cluster and suppresses (-) the expression of the emericellamide (*eas*) gene cluster. Only the presence of AdaB and GcnE in the Saga/Ada complex has been experimentally proven yet.

Supplementary Material

Supplemental Results

Details of the ChIP analysis

After first examination, we found that a significant proportion of co-incubated library reads originated from *S. rapamycinicus*. A fused genome concatenating the *A. nidulans* and the *S. rapamycinicus* genomes was generated. We found that about 90-98% of the reads mapped against the fused genome (Table S1), which suggested a high quality of sequencing data. This assumption was confirmed by examining the quality of libraries using FastQC (data not shown). As indicated, the coverage was substantially higher on the *S. rapamycinicus* genome with only ~20 % mapping to the *A. nidulans* genome (see Table S1). Expectedly, this ratio has shifted considerably towards *A. nidulans* genome for histone targeting ChIP libraries (Fig. 1 A, panel 2 - 4) going up from 20 % to around 90 % for all H3, H3K9 and H314 libraries validating correct antibody enrichment as *S. rapamycinicus* is devoid of histones. However around 10 % of reads were still mapping to the *S. rapamycinicus* genome which might be due to imperfect antibody specificity. Coverage depth deviations were accounted for by only considering reads originating from *A. nidulans*. This allowed for calculation of library size factors used for library normalization. To assess antibody specificity, we calculated the fraction of reads mapping to mitochondria, which do not contain histones. The control library amounted to about 1.2 % of reads as opposed to about 2-5 % for H3, H3K9ac, H3K14ac libraries constituting 40-50 fold enrichment. In an effort to determine binding sites of GcnE during the microbial interaction, a strain harboring a 3xC-term-FLAG-tagged-GcnE was used in all conducted experiments. However, the mapping rates obtained for the ChIP-seq experiment with an antibody against FLAG-tag were too low and therefore excluded from the data analysis. As a background control we used ChIP material obtained from anti-

FLAG-tag antibody precipitates of a non-tagged fungal wild-type strain co-cultivated under the same conditions with *S. rapamycinicus.*

Changes of H3K9 and H3K14 acetylation profiles in *A. nidulans* in response to *S. rapamycinicus*

As reported in the manuscript, the genome-wide H3K9 and H3K14 chromatin landscape of *A. nidulans* was determined. There was also a drop-off in all libraries at the chromosome arms, which was most likely caused by the bordering bins being shorter and therefore account for less reads. As the gene density varies across the genome, spearman correlation was calculated to correlate the read counts and the gene counts among the 50k bins. As expected, there was almost no correlation between the background and the genes (r = 0.09). However, for H3 we found it to be rather high (r = 0.37). Since the used bin size is large, this could point at global H3 occupancy to be higher for high gene density regions such as euchromatin and low H3 occupancy for heterochromatin. Noteworthy, the correlation between read and gene density was found to be lower for H3K14ac and H3K9ac (r=0.14 and 0.15 respectively), which might indicate a more subtle regulatory mechanism for those marks targeting individual genes as opposed to larger domains. Notably, the highest correlation was found between the two acetylation marks (r=0.57) hinting at some potential cross-talk or common regulation between them.

Figure S1. Correlation of data points for LFCs of ChIP-seq with LFCs of microarray data for all *A. nidulans* genes, depicting single data points and the correlation coefficient.

Figure S2. Pairwise comparison of ChIP-seq and microarray intensities of all genes in *A. nidulans* monoculture. The numbers resemble the correlation coefficient for the respective comparison. Intensity defines enrichment of number of reads per gene.

Figure S3. Histone H3 normalized read count frequencies for H3K9ac (green) and K14 ac (blue) at the (A) TSS and (B) TTS. The enrichment is given in signal to H3 ratio. Multiple lines per ChIP target resemble the three independent biological replicates.

Figure S4. Density plot of TSS (A, C, E) and TTS (B, D, F) given for different gene expression levels (q1-q4). (**A**, **B**) Specific enrichment of H3K9ac, (**C**, **D**) H3K14ac and (**E**, **F**) H3 is given in read count frequency. Thereby q1 are the lower 25 %, q2 the medium lower 25 – 50 %, q3 are the medium high 50-75 %, q4 higher 25 %.

Figure S5. Generation of *cpcA* deletion mutant and impact on the *ors* gene cluster induction in response to *S. rapamycinicus*. (**A**) Chromsomal organization of the *A. nidulans* *cpcA* gene before and after deletion. The *cpcA* gene was replaced by an *argB* cassette in *A. nidulans* wild-type strain A1153. Genomic DNA was digested with *Nhe*I. A PCR fragment covering the downstream sequence of *cpcA* was used as a probe (*). wt, wild-type strain as a control. (**B**) LC-MS-based detection of orsellinic acid (1) and lecanoric acid (2) in the co-cultivation of the *cpcA* deletion mutant and *S. rapamycinicus*.

Figure S6. Molecular phylogenetic analysis of BasR (*AN7174*). The tree reports distances between BasR-similar amino acid sequences identified by BlastP analysis using the entire sequences. The percentage of trees in which the associated taxa clustered together is shown next to the branches. The BasR proteins from *A. nidulans*, *A. calidoustus*, *A. sydowii*, *A. versicolor*, *A. rambellii* and *A. ochraceoroseus* form a separate clade (reported in purple), while the yeast Bas1-related sequences are more distantly related to BasR (in red). The

second similar Myb-like transcription factor from *A. nidulans* (*AN8377*) forms a clade with orthologues from *A. calidoustus* and *A. versicolor* (in blue), which seems to be more related to Bas1 than to BasR. The names of the selected sequences are given according to their UniProt accession numbers.

Figure S7. Generation of a *basR* deletion mutant and inducible overexpression strain based on the *A. nidulans* wild-type strain A1153. (**A**) Genomic organization of *basR* and Southern blot analysis of *basR* deletion. The *basR* gene was replaced by the *argB* gene. Transformant strains were checked with a probe (*) directed against the flanking region of the construct. Genomic DNA was digested with *Cla*I. wt, wild-type strain as a control. (**B**) Generation of the inducible *basR* overexpression strain by complementation of the *basR* deletion strain. The *tet*^{On}-*basR* gene cassette was integrated at the Δ*basR* genomic locus using the *pabA1* gene as selectable marker replacing the *argB* marker. The genomic DNA was cut with *Bam*HI. Transformant strains were checked with a probe (*) directed against the flanking region of the construct.

Figure S8. Generation of the inducible *basR* overexpression strain by ectopic integration of an additional copy of the *basR* gene in the *A. sydowii* wild-type strain (wt). The *tet*^{On}-*basR* construct was integrated ectopically into the wild-type genome, using the *hph* cassette as selectable marker. For Southern blot analysis, transformant strains were checked with a probe (*) directed against a region flanking the *tet*^{On} cassette and *basR* gene. The genomic DNA was digested with *Bam*HI.

Table S1. Summary of ChIP-seq data

Table S2. List of primers used in this study.

References

AIYAR, P., SCHAEME, D., GARCÍA-ALTARES, M., CARRASCO-FLORES, D., DATHE, H., HERTWECK, C., SASSO, S. & MITTAG, M. 2017. Antagonistic bacteria disrupt calcium homeostasis and immobilize algal cells. *Nat. Commun.*, in press.

ALLSHIRE, R. C. & EKWALL, K. 2015. Epigenetic regulation of chromatin states in *Schizosaccharomyces pombe*. *Cold Spring Harbor Perspect. Biol.,* 7**,** a018770.

ARAÚJO, F. D. D. S., ARAÚJO, W. L. & EBERLIN, M. N. 2017. Potential of *Burkholderia seminalis* TC3.4.2R3 as biocontrol agent against *Fusarium oxysporum* evaluated by mass spectrometry imaging. *J. Am. Soc. Mass. Spectrom.,* 28**,** 901-907.

BAKER, S. P. & GRANT, P. A. 2007. The SAGA continues: expanding the cellular role of a transcriptional co-activator complex. *Oncogene,* 26**,** 5329-5340.

BALLANCE, D. J. & TURNER, G. 1985. Development of a high-frequency transforming vector for *Aspergillus nidulans*. *Gene,* 36**,** 321-31.

BANNISTER, A. J. & KOUZARIDES, T. 2011. Regulation of chromatin by histone modifications. *Cell Res.,* 21**,** 381-395.

BERGER, H., BASHEER, A., BÖCK, S., REYES-DOMINGUEZ, Y., DALIK, T., ALTMANN, F. & STRAUSS, J. 2008. Dissecting individual steps of nitrogen transcription factor cooperation in the *Aspergillus nidulans* nitrate cluster. *Mol. Microbiol.,* 69**,** 1385-1398.

BRAKHAGE, A. A. 2013. Regulation of fungal secondary metabolism. *Nat. Rev. Microbiol.,* 11**,** 21-32.

BRAKHAGE, A. A. & VAN DEN BRULLE, J. 1995. Use of reporter genes to identify recessive trans-acting mutations specifically involved in the regulation of *Aspergillus nidulans* penicillin biosynthesis genes. *J. Bacteriol.,* 177**,** 2781-2788.

CÁNOVAS, D., MARCOS, A. T., GACEK, A., RAMOS, M. S., GUTIÉRREZ, G., REYES-DOMÍNGUEZ, Y. & STRAUSS, J. 2014. The histone acetyltransferase GcnE (GCN5) plays a central role in the regulation of *Aspergillus* asexual development. *Genetics,* 197**,** 1175-1189.

CUETO, M., JENSEN, P. R., KAUFFMAN, C., FENICAL, W., LOBKOVSKY, E. & CLARDY, J. 2001. Pestalone, a new antibiotic produced by a marine fungus in response to bacterial challenge. *J. Nat. Prod.,* 64**,** 1444-1446.

DAIGNAN-FORNIER, B. & FINK, G. R. 1992. Coregulation of purine and histidine biosynthesis by the transcriptional activators BAS1 and BAS2. *PNAS,* 89**,** 6746-6750.

DEMENTHON, K., PAOLETTI, M., PINAN-LUCARRÉ, B., LOUBRADOU-BOURGES, N., SABOURIN, M., SAUPE, S. J. & CLAVÉ, C. 2003. Rapamycin mimics the incompatibility reaction in the fungus *Podospora anserina*. *Eukaryot Cell,* 2**,** 238-246.

DOCIMO, T., REICHELT, M., SCHNEIDER, B., KAI, M., KUNERT, G., GERSHENZON, J. & D'AURIA, J. C. 2012. The first step in the biosynthesis of cocaine in *Erythroxylum coca*: the characterization of arginine and ornithine decarboxylases. *Plant Mol. Biol.,* 78**,** 599-615.

DOWNEY, M., JOHNSON, J. R., DAVEY, N. E., NEWTON, B. W., JOHNSON, T. L., GALAANG, S., SELLER, C. A., KROGAN, N. & TOCZYSKI, D. P. 2015. Acetylome profiling reveals overlap in the regulation of diverse processes by sirtuins, Gcn5, and Esa1. *Mol. Cell. Proteomics,* 14**,** 162-176.

EDGAR, R. C. 2004. MUSCLE: multiple sequence alignment with high accuracy and high throughput. *Nucleic Acids Res.* , 32**,** 1792-1797.

EIYAMA, A., KONDO-OKAMOTO, N. & OKAMOTO, K. 2013. Mitochondrial degradation during starvation is selective and temporally distinct from bulk autophagy in yeast. *FEBS Lett.,* 587**,** 1787-1792.

EKBLOM, R. & WOLF, J. B. W. 2014. A field guide to whole-genome sequencing, assembly and annotation. *Evol. Appl.,* 7**,** 1026-1042.

FENG, G. H. & LEONARD, T. J. 1998. Culture conditions control expression of the genes for aflatoxin and sterigmatocystin biosynthesis in *Aspergillus parasiticus* and *A. nidulans*. *Appl. Environ. Microbiol.* , 64**,** 2275-2277.

941 GACEK-MATTHEWS, A., BERGER, H., SASAKI, T., WITTSTEIN, K., GRUBER, C., LEWIS, Z. A. &
942 STRAUSS, J. 2016. KdmB, a jumonji histone H3 demethylase, regulates genome-wide H3K4
943 trimethylation and is required for normal induction of secondary metabolism in *Aspergillus*
944 *nidulans*. *PLos Genet.,* 12**,** e1006222.
945 GACEK, A. & STRAUSS, J. 2012. The chromatin code of fungal secondary metabolite gene clusters.
946 *Appl. Microbiol. Biotechnol.,* 95**,** 1389-1404.
947 GEL, B., DÍEZ-VILLANUEVA, A., SERRA, E., BUSCHBECK, M., PEINADO, M. A. & MALINVERNI, R. 2016.
948 regioneR: an R/Bioconductor package for the association analysis of genomic regions based
949 on permutation tests. *Bioinformatics,* 32**,** 289-291.
950 GROSSO, A. R., DE ALMEIDA, S. F., BRAGA, J. & CARMO-FONSECA, M. 2012. Dynamic transitions in
951 RNA polymerase II density profiles during transcription termination. *Genome Res.,* 22**,** 1447-
952 1456.
953 HAYNES, B. C., SKOWYRA, M. L., SPENCER, S. J., GISH, S. R., WILLIAMS, M., HELD, E. P., BRENT, M. R. &
954 DOERING, T. L. 2011. Toward an integrated model of capsule regulation in *Cryptococcus*
955 *neoformans*. *PLoS Pathog.,* 7**,** e1002411.
956 HELMSCHROTT, C., SASSE, A., SAMANTARAY, S., KRAPPMANN, S. & WAGENER, J. 2013. Upgrading
957 fungal gene expression on demand: improved systems for doxycycline-dependent silencing in
958 *Aspergillus fumigatus*. *Appl. Environ. Microbiol.,* 79**,** 1751-1754.
959 HOFFMANN, T. & DORRESTEIN, P. C. 2015. Homogeneous matrix deposition on dried agar for MALDI
960 imaging mass spectrometry of microbial cultures. *J. Am. Soc. Mass. Spectrom.,* 26**,** 1959-
961 1962.
962 JIANG, C. & PUGH, B. F. 2009. Nucleosome positioning and gene regulation: advances through
963 genomics. *Nat. Rev. Genet.,* 10**,** 161-172.
964 KANKI, T. & KLIONSKY, D. J. 2008. Mitophagy in yeast occurs through a selective mechanism. *J. Biol.*
965 *Chem.,* 283**,** 32386-32393.
966 KAPLAN, N., MOORE, I., FONDUFE-MITTENDORF, Y., GOSSETT, A. J., TILLO, D., FIELD, Y., HUGHES, T.
967 R., LIEB, J. D., WIDOM, J. & SEGAL, E. 2010. Nucleosome sequence preferences influence in
968 vivo nucleosome organization. *Nat. Struct. Mol. Biol.* , 17**,** 918-922.
969 KAZAN, K., GARDINER, D. M. & MANNERS, J. M. 2012. On the trail of a cereal killer: recent advances
970 in *Fusarium graminearum* pathogenomics and host resistance. *Mol. Plant Pathol,* 13**,** 399-
971 413.
972 KELLER, N. P. 2015. Translating biosynthetic gene clusters into fungal armor and weaponry. *Nat.*
973 *Chem. Biol.,* 11**,** 671-677.
974 KIESER, T., BIBB, M. J., BUTTNER, M. J., CHATER, K. F. & HOPWOOD, D. A. 2000. *Practical Streptomyes*
975 *genetics,* Norwich, United Kingdom, John Innes Foundation.
976 KIM, Y., ISLAM, N., MOSS, B. J., NANDAKUMAR, M. P. & MARTEN, M. R. 2011. Autophagy induced by
977 rapamycin and carbon-starvation have distinct proteome profiles in *Aspergillus nidulans*.
978 *Biotechnol. Bioeng.* , 108**,** 2705-2715.
979 KRAPPMANN, S. & BRAUS, G. H. 2005. Nitrogen metabolism of *Aspergillus* and its role in
980 pathogenicity. *Med. Mycol.,* 43**,** S31-S40.
981 KUMAR, Y. & GOODFELLOW, M. 2008. Five new members of the *Streptomyces violaceusniger* 16S
982 rRNA gene clade: *Streptomyces castelarensis* sp. nov., comb. nov., *Streptomyces*
983 *himastatinicus* sp. nov., *Streptomyces mordarskii* sp. nov., *Streptomyces rapamycinicus* sp.
984 nov. and *Streptomyces ruanii* sp. nov. *Int. J. Syst. Evol. Microbiol.* , 58**,** 1369-78.
985 MACHELEIDT, J., MATTERN, D. J., FISCHER, J., NETZKER, T., WEBER, J., SCHROECKH, V., VALIANTE, V. &
986 BRAKHAGE, A. A. 2016. Regulation and role of fungal secondary metabolites. *Annu. Rev.*
987 *Genet.,* 50**,** 371-392.
988 MEWS, P., ZEE, B. M., LIU, S., DONAHUE, G., GARCIA, B. A. & BERGER, S. L. 2014. Histone methylation
989 has dynamics distinct from those of histone acetylation in cell cycle reentry from quiescence.
990 *Mol. Cell. Biol.,* 34**,** 3968-3980.
991 NAYAK, T., SZEWCZYK, E., OAKLEY, C. E., OSMANI, A., UKIL, L., MURRAY, S. L., HYNES, M. J., OSMANI,
992 S. A. & OAKLEY, B. R. 2006. A versatile and efficient gene-targeting system for *Aspergillus*
993 *nidulans*. *Genetics,* 172**,** 1557-1566.

NETZKER, T., FISCHER, J., WEBER, J., MATTERN, D. J., KÖNIG, C. C., VALIANTE, V., SCHROECKH, V. & BRAKHAGE, A. A. 2015. Microbial communication leading to the activation of silent fungal secondary metabolite gene clusters. *Front. Microbiol.,* 6**,** 299.

NIEHAUS, E.-M., VON BARGEN, K. W., ESPINO, J. J., PFANNMÜLLER, A., HUMPF, H.-U. & TUDZYNSKI, B. 2014. Characterization of the fusaric acid gene cluster in *Fusarium fujikuroi*. *Appl. Microbiol. Biotechnol.,* 98**,** 1749-1762.

NÜTZMANN, H.-W., FISCHER, J., SCHERLACH, K., HERTWECK, C. & BRAKHAGE, A. A. 2013. Distinct amino acids of histone H3 control secondary metabolism in *Aspergillus nidulans*. *Appl. Environ. Microbiol.,* 79**,** 6102-6109.

NÜTZMANN, H.-W., REYES-DOMINGUEZ, Y., SCHERLACH, K., SCHROECKH, V., HORN, F., GACEK, A., SCHÜMANN, J., HERTWECK, C., STRAUSS, J. & BRAKHAGE, A. A. 2011. Bacteria-induced natural product formation in the fungus *Aspergillus nidulans* requires Saga/Ada-mediated histone acetylation. *PNAS,* 108**,** 14282-14287.

PENN, M. D., GALGOCI, B. & GREER, H. 1983. Identification of AAS genes and their regulatory role in general control of amino acid biosynthesis in yeast. *PNAS,* 80**,** 2704-2708.

PINSON, B., KONGSRUD, T. L., ORDING, E., JOHANSEN, L., DAIGNAN-FORNIER, B. & GABRIELSEN, O. S. 2000. Signaling through regulated transcription factor interaction: mapping of a regulatory interaction domain in the Myb-related Bas1p. *Nucleic Acids Res.,* 28**,** 4665-4673.

ROBINSON, M. D. & OSHLACK, A. 2010. A scaling normalization method for differential expression analysis of RNA-seq data. *Genome Biol.,* 11**,** R25.

SACHS, M. S. 1996. General and cross-pathway controls of amino acid biosynthesis. *In:* BRAMBL, R. & MARZLUF, G. A. (eds.) *Biochemistry and Molecular Biology.* Berlin, Heidelberg: Springer Berlin Heidelberg.

SCHERLACH, K. & HERTWECK, C. 2009. Triggering cryptic natural product biosynthesis in microorganisms. *Org. Biomol. Chem.* , 7**,** 1753-1760.

SCHERLACH, K., SARKAR, A., SCHROECKH, V., DAHSE, H.-M., ROTH, M., BRAKHAGE, A. A., HORN, U. & HERTWECK, C. 2011. Two induced fungal polyketide pathways converge into antiproliferative spiroanthrones. *ChemBioChem,* 12**,** 1836-1839.

SCHERLACH, K., SCHUEMANN, J., DAHSE, H.-M. & HERTWECK, C. 2010. Aspernidine A and B, prenylated isoindolinone alkaloids from the model fungus *Aspergillus nidulans*. *J. Antibiot.,* 63**,** 375-377.

SCHROECKH, V., SCHERLACH, K., NÜTZMANN, H. W., SHELEST, E., SCHMIDT-HECK, W., SCHUEMANN, J., MARTIN, K., HERTWECK, C. & BRAKHAGE, A. A. 2009. Intimate bacterial-fungal interaction triggers biosynthesis of archetypal polyketides in *Aspergillus nidulans*. *PNAS,* 106**,** 14558-63.

SMITH, K. M., PHATALE, P. A., SULLIVAN, C. M., POMRANING, K. R. & FREITAG, M. 2011. Heterochromatin is required for normal distribution of *Neurospora crassa* CenH3. *Mol. Cell. Biol.,* 31**,** 2528-2542.

SPRINGER, C., KÜNZLER, M., BALMELLI, T. & BRAUS, G. H. 1996. Amino acid and adenine cross-pathway regulation act through the same 5'-TGACTC-3' motif in the yeast HIS7 promoter. *J. Biol. Chem.,* 271**,** 29637-29643.

STACK, D., NEVILLE, C. & DOYLE, S. 2007. Nonribosomal peptide synthesis in *Aspergillus fumigatus* and other fungi. *Microbiology,* 153**,** 1297-1306.

STUDT, L., SCHMIDT, F. J., JAHN, L., SIEBER, C. M. K., CONNOLLY, L. R., NIEHAUS, E. M., FREITAG, M., HUMPF, H. U. & TUDZYNSKI, B. 2013. Two histone deacetylases, FfHda1 and FfHda2, are important for *Fusarium fujikuroi s*econdary metabolism and virulence. *Appl. Environ. Microbiol.,* 79**,** 7719-7734.

STUDT, L., WIEMANN, P., KLEIGREWE, K., HUMPF, H.-U. & TUDZYNSKI, B. 2012. Biosynthesis of fusarubins accounts for pigmentation of *Fusarium fujikuroi* perithecia. *Appl. Environ. Microbiol.,* 78**,** 4468-4480.

SZEWCZYK, E., NAYAK, T., OAKLEY, C. E., EDGERTON, H., XIONG, Y., TAHERI-TALESH, N., OSMANI, S. A. & OAKLEY, B. R. 2007. Fusion PCR and gene targeting in *Aspergillus nidulans*. *Nat. Protoc.,* 1**,** 3111-3120.

TAMURA, K., STECHER, G., PETERSON, D., FILIPSKI, A. & KUMAR, S. 2013. MEGA6: molecular evolutionary genetics analysis version 6.0. *Mol. Biol. Evol.,* 30**,** 2725-2729.

THORVALDSDÓTTIR, H., ROBINSON, J. T. & MESIROV, J. P. 2013. Integrative genomics viewer (IGV): high-performance genomics data visualization and exploration. *Briefings Bioinf.,* 14**,** 178-192.

TUDZYNSKI, B. 2014. Nitrogen regulation of fungal secondary metabolism in fungi. *Front. Microbiol.,* 5**,** 656.

VALERIUS, O., BRENDEL, C., WAGNER, C., KRAPPMANN, S., THOMA, F. & BRAUS, G. H. 2003. Nucleosome position-dependent and -independent activation of *HIS7* expression in *Saccharomyces cerevisiae* by different transcriptional activators. *Eukaryot Cell,* 2**,** 876-885.

WATERS, R., VAN EIJK, P. & REED, S. 2015. Histone modification and chromatin remodeling during NER. *DNA Repair,* 36**,** 105-113.

WIEMANN, P. & KELLER, N. P. 2014. Strategies for mining fungal natural products. *J Ind Microbiol Biotechnol,* 41**,** 301-313.

WIEMANN, P., SIEBER, C. M. K., VON BARGEN, K. W., STUDT, L., NIEHAUS, E.-M., ESPINO, J. J., HUß, K., MICHIELSE, C. B., ALBERMANN, S., WAGNER, D., BERGNER, S. V., CONNOLLY, L. R., FISCHER, A., REUTER, G., KLEIGREWE, K., BALD, T., WINGFIELD, B. D., OPHIR, R., FREEMAN, S., HIPPLER, M., SMITH, K. M., BROWN, D. W., PROCTOR, R. H., MÜNSTERKÖTTER, M., FREITAG, M., HUMPF, H.-U., GÜLDENER, U. & TUDZYNSKI, B. 2013. Deciphering the cryptic genome: genome-wide analyses of the rice pathogen *Fusarium fujikuroi* reveal complex regulation of secondary metabolism and novel metabolites. *PLoS Pathog.,* 9**,** e1003475.

YU, G., WANG, L.-G. & HE, Q.-Y. 2015. ChIPseeker: an R/Bioconductor package for ChIP peak annotation, comparison and visualization. *Bioinformatics,* 31**,** 2382-2383.

ZHANG, F., KIROUAC, M., ZHU, N., HINNEBUSCH, A. G. & ROLFES, R. J. 1997. Evidence that complex formation by Bas1p and Bas2p (Pho2p) unmasks the activation function of Bas1p in an adenine-repressible step of ADE gene transcription. *Mol. Cell. Biol.,* 17**,** 3272-3283.

ZHANG, Y., LIU, T., MEYER, C. A., EECKHOUTE, J., JOHNSON, D. S., BERNSTEIN, B. E., NUSBAUM, C., MYERS, R. M., BROWN, M., LI, W. & LIU, X. S. 2008. Model-based Analysis of ChIP-Seq (MACS). *Genome Biol.,* 9**,** R137-R137.

1096 **Figures**

1097

1098

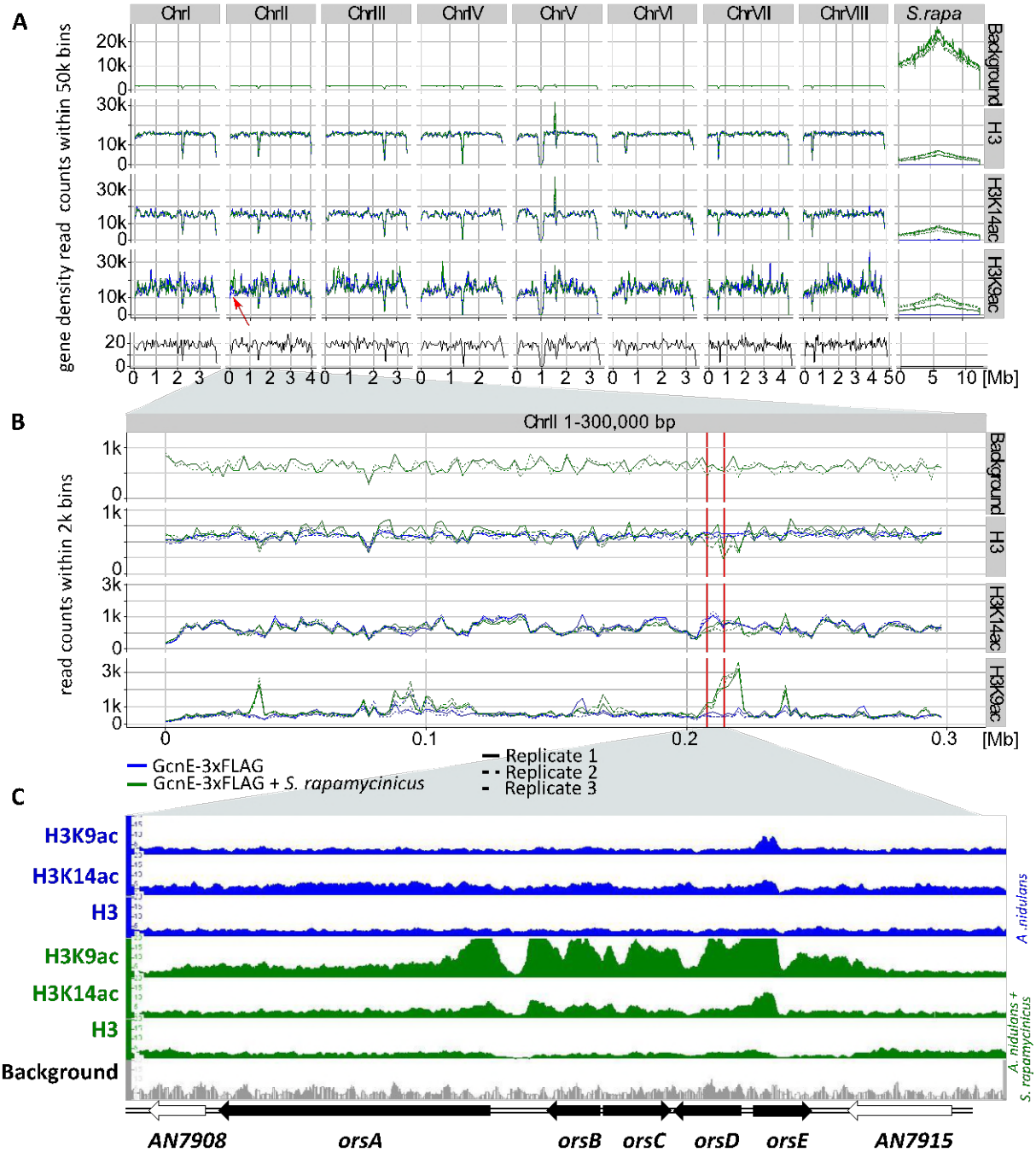

1099

1100 **Figure 1**

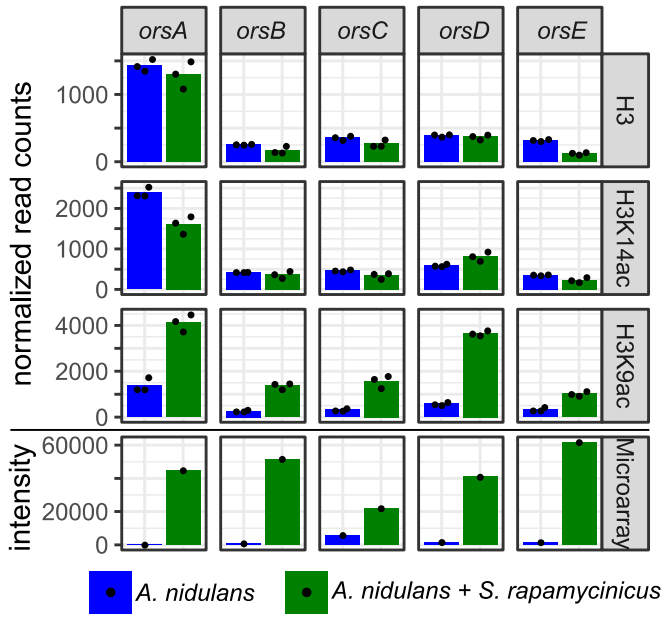

Figure 2

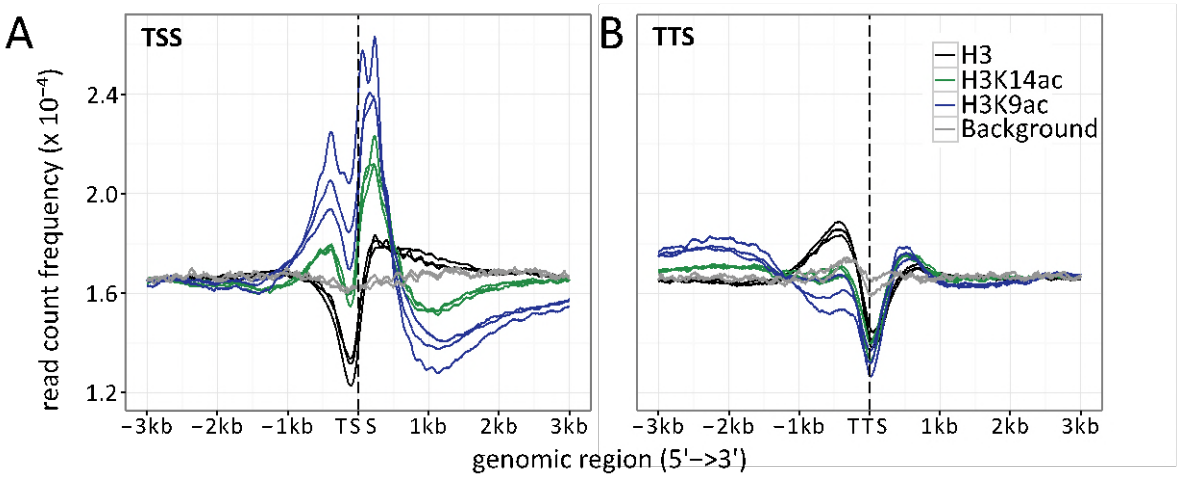

Figure 3

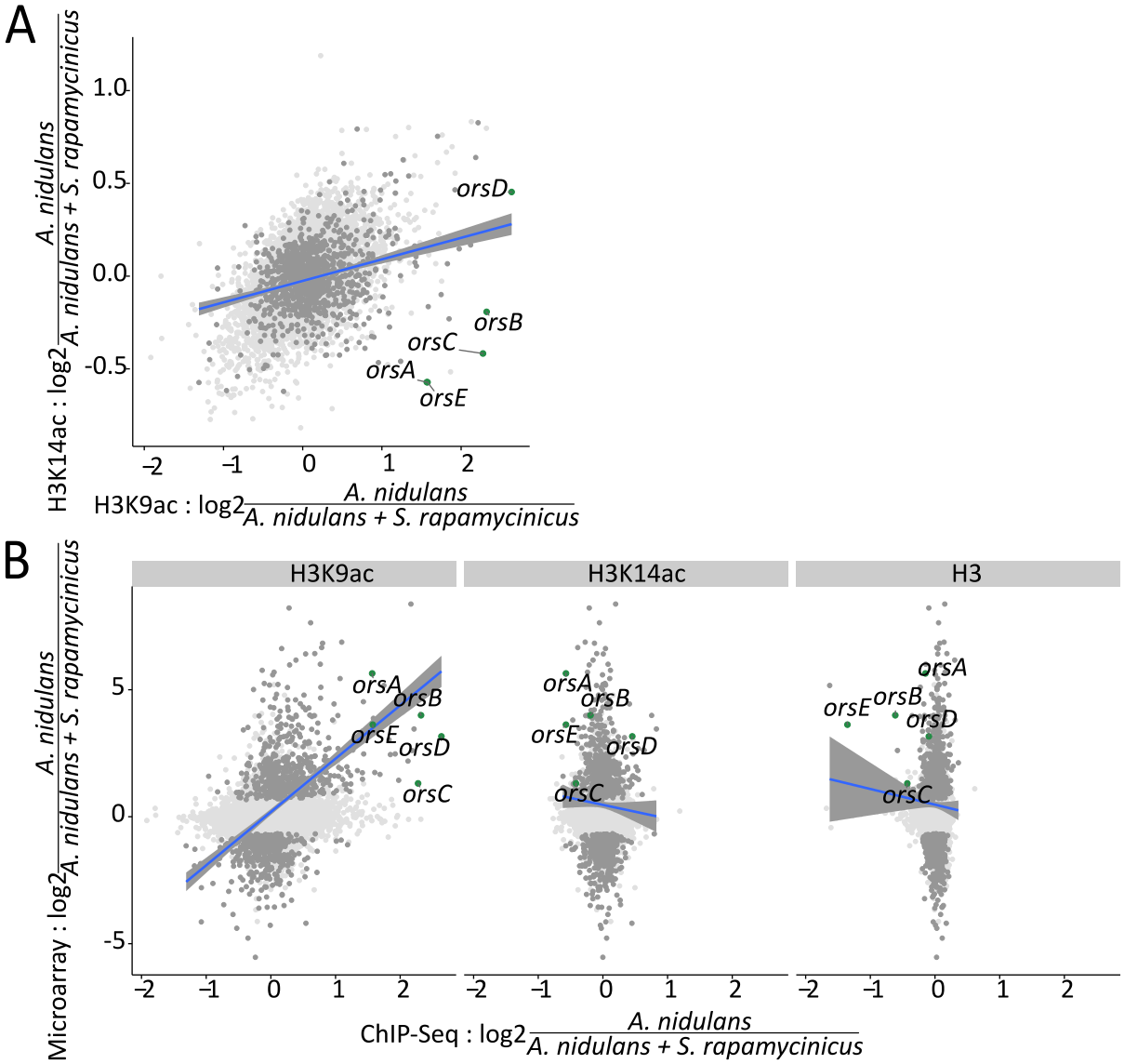

Figure 4

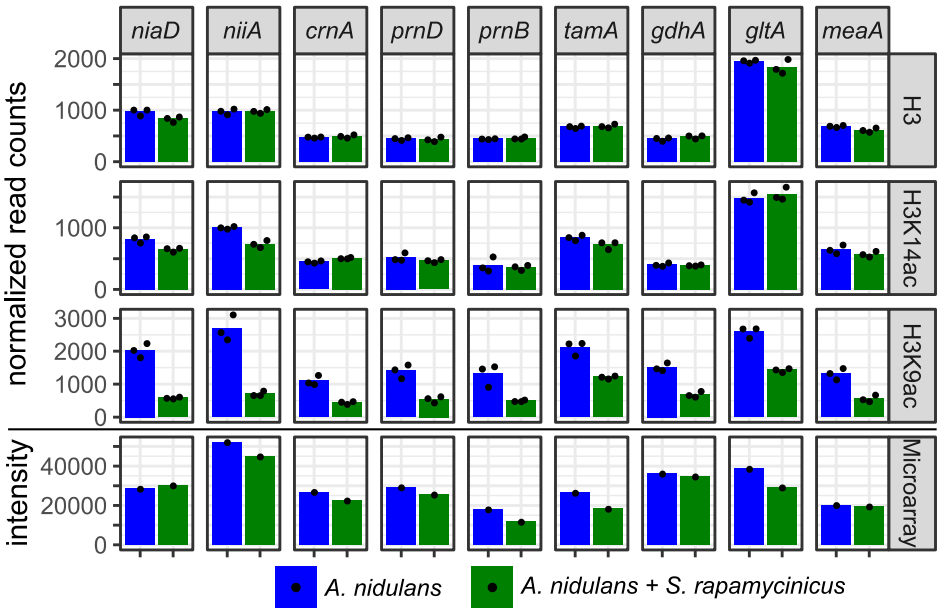

1115

1116 **Figure 5**

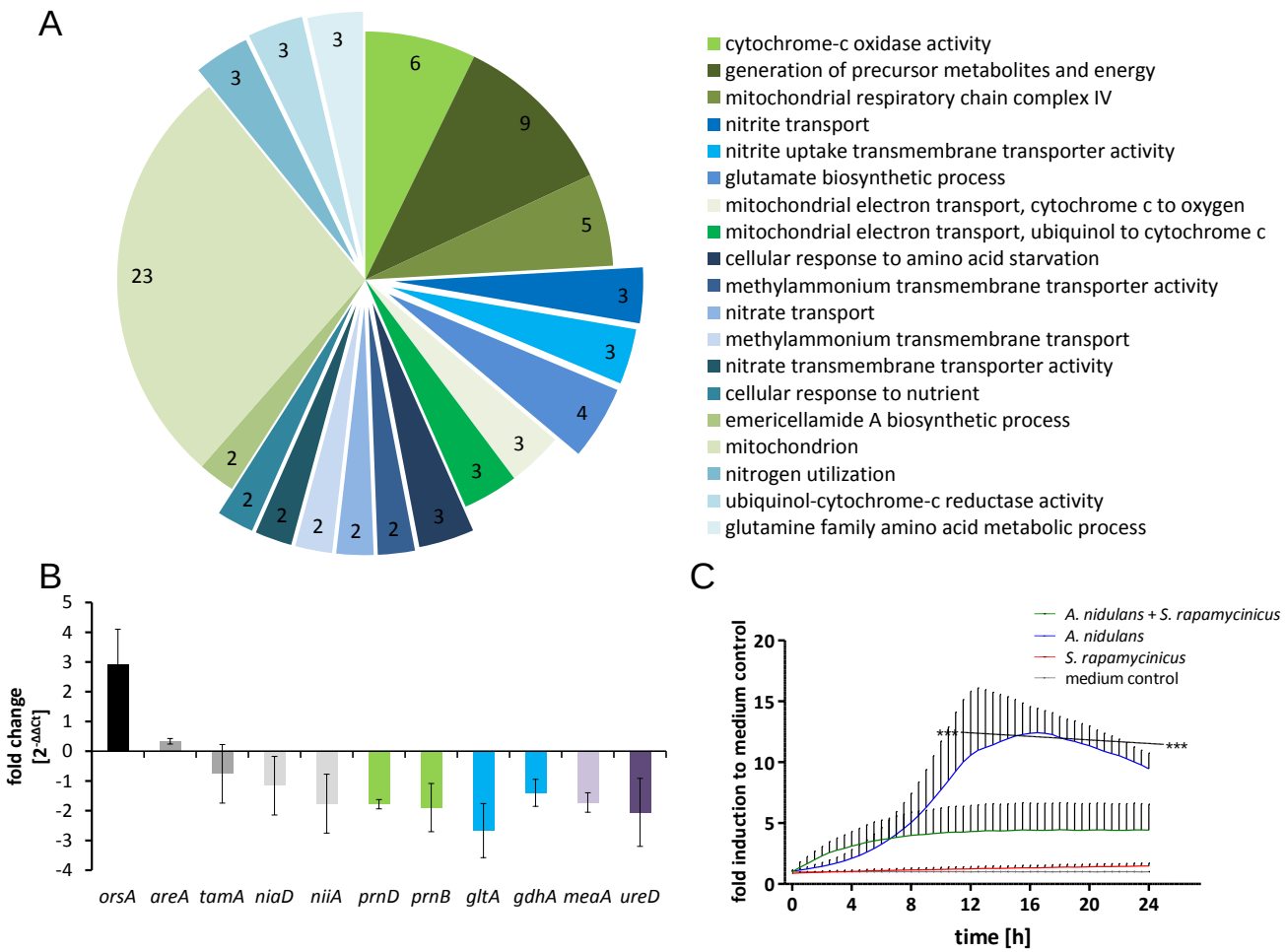

1117

1118 **Figure 6**

1119

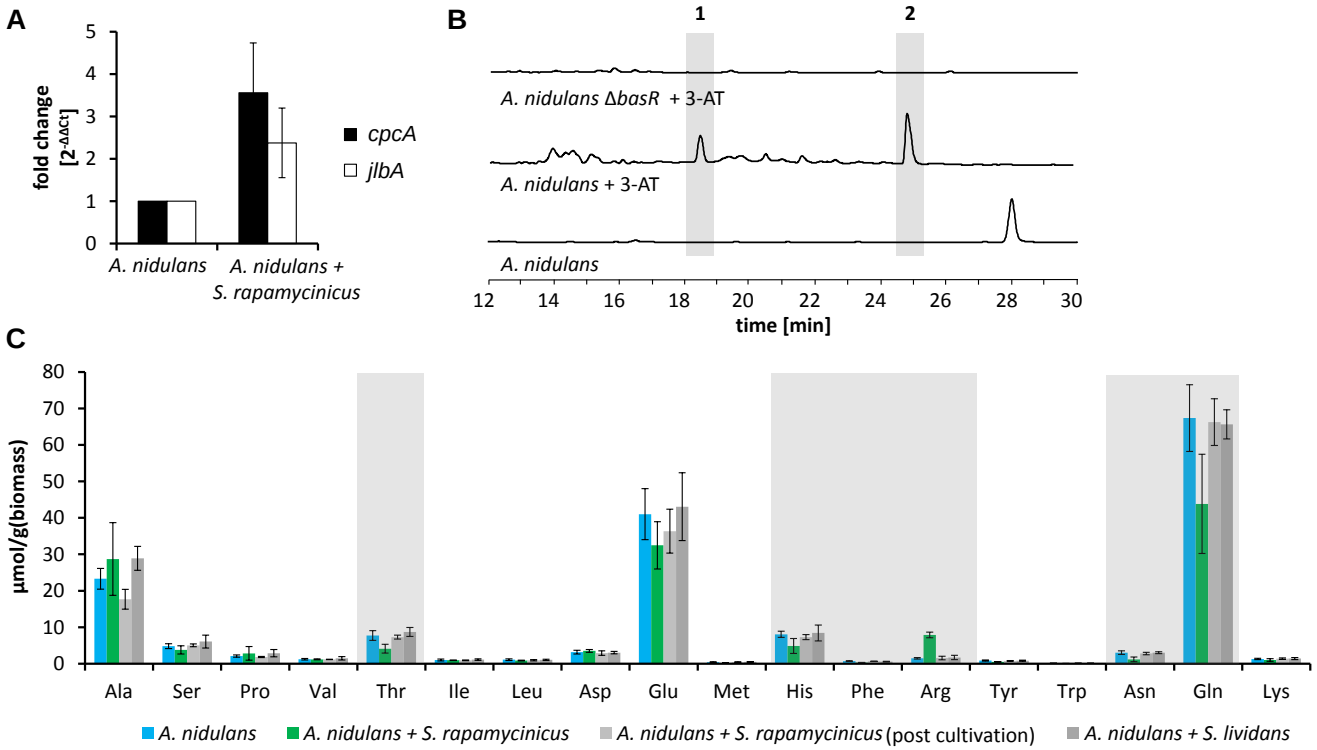
A
fold change [2^-ΔΔCt]
cpcA
jlbA
A. nidulans
A. nidulans + S. rapamycinicus
B
1
2
A. nidulans ΔbasR + 3-AT
A. nidulans + 3-AT
A. nidulans
time [min]
C
µmol/g(biomass)
Ala Ser Pro Val Thr Ile Leu Asp Glu Met His Phe Arg Tyr Trp Asn Gln Lys
A. nidulans
A. nidulans + S. rapamycinicus
A. nidulans + S. rapamycinicus (post cultivation)
A. nidulans + S. lividans

Figure 7

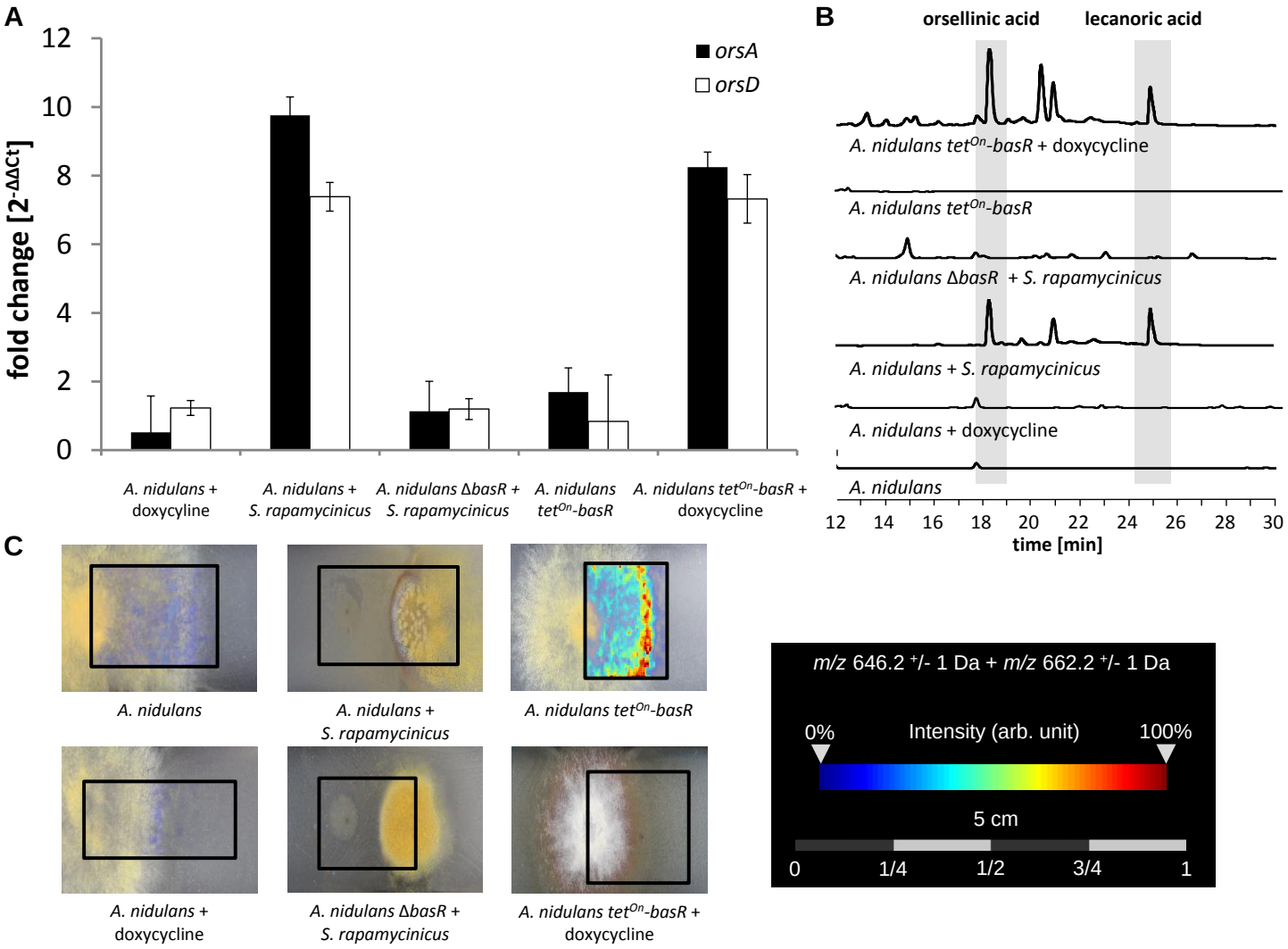
A
fold change [2-ΔΔCt]
orsA
orsD
A. nidulans + doxycyline
A. nidulans + S. rapamycinicus
A. nidulans ΔbasR + S. rapamycinicus
A. nidulans tetOn-basR
A. nidulans tetOn-basR + doxycycline
B
orsellinic acid
lecanoric acid
A. nidulans tetOn-basR + doxycycline
A. nidulans tetOn-basR
A. nidulans ΔbasR + S. rapamycinicus
A. nidulans + S. rapamycinicus
A. nidulans + doxycycline
A. nidulans
time [min]
C
A. nidulans
A. nidulans + S. rapamycinicus
A. nidulans tetOn-basR
A. nidulans + doxycycline
A. nidulans ΔbasR + S. rapamycinicus
A. nidulans tetOn-basR + doxycycline
m/z 646.2 +/- 1 Da + m/z 662.2 +/- 1 Da
0%
Intensity (arb. unit)
100%
5 cm
0
1/4
1/2
3/4
1

Figure 8

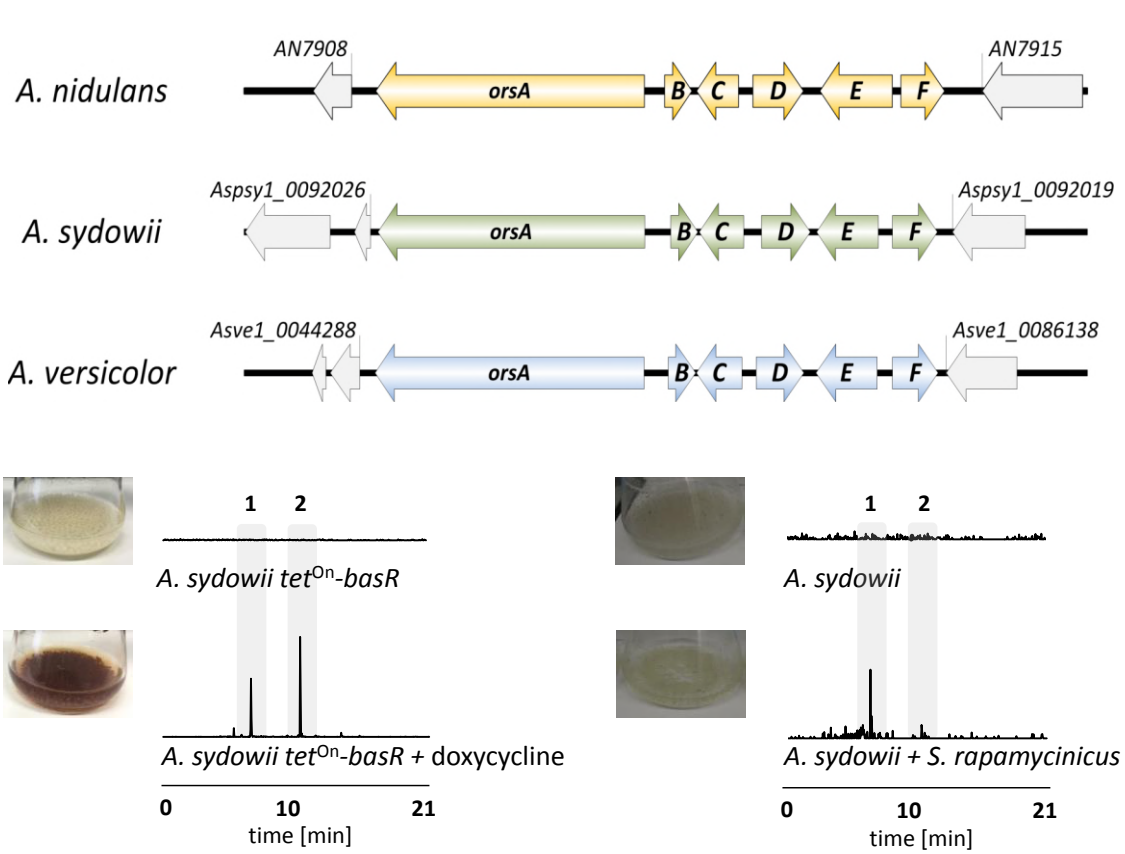

Figure 9

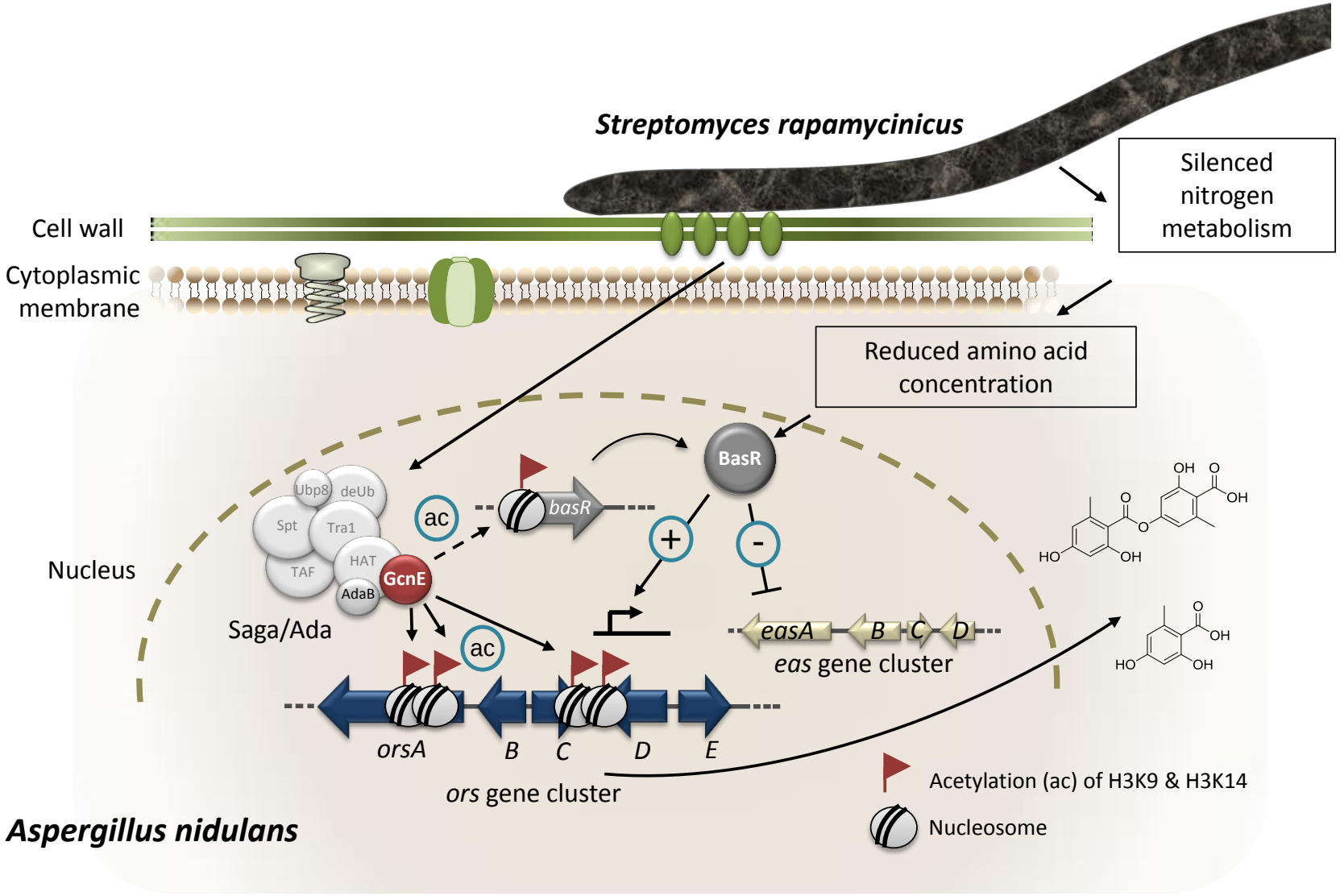
Streptomyces rapamycinicus
Silenced nitrogen metabolism
Cell wall
Cytoplasmic membrane
Reduced amino acid concentration
Nucleus
BasR
basR
ac
+
-
Ubp8
deUb
Spt
Tra1
HAT
TAF
GcnE
AdaB
Saga/Ada
ac
easA
B
C
D
eas gene cluster
orsA
B
C
D
E
ors gene cluster
Aspergillus nidulans
Acetylation (ac) of H3K9 & H3K14
Nucleosome

Figure 10

1131

ChIP-seq/ Microarray log_2 fold change for all genes:
A. nidulans vs. *A. nidulans* + *S. rapamycinicus*

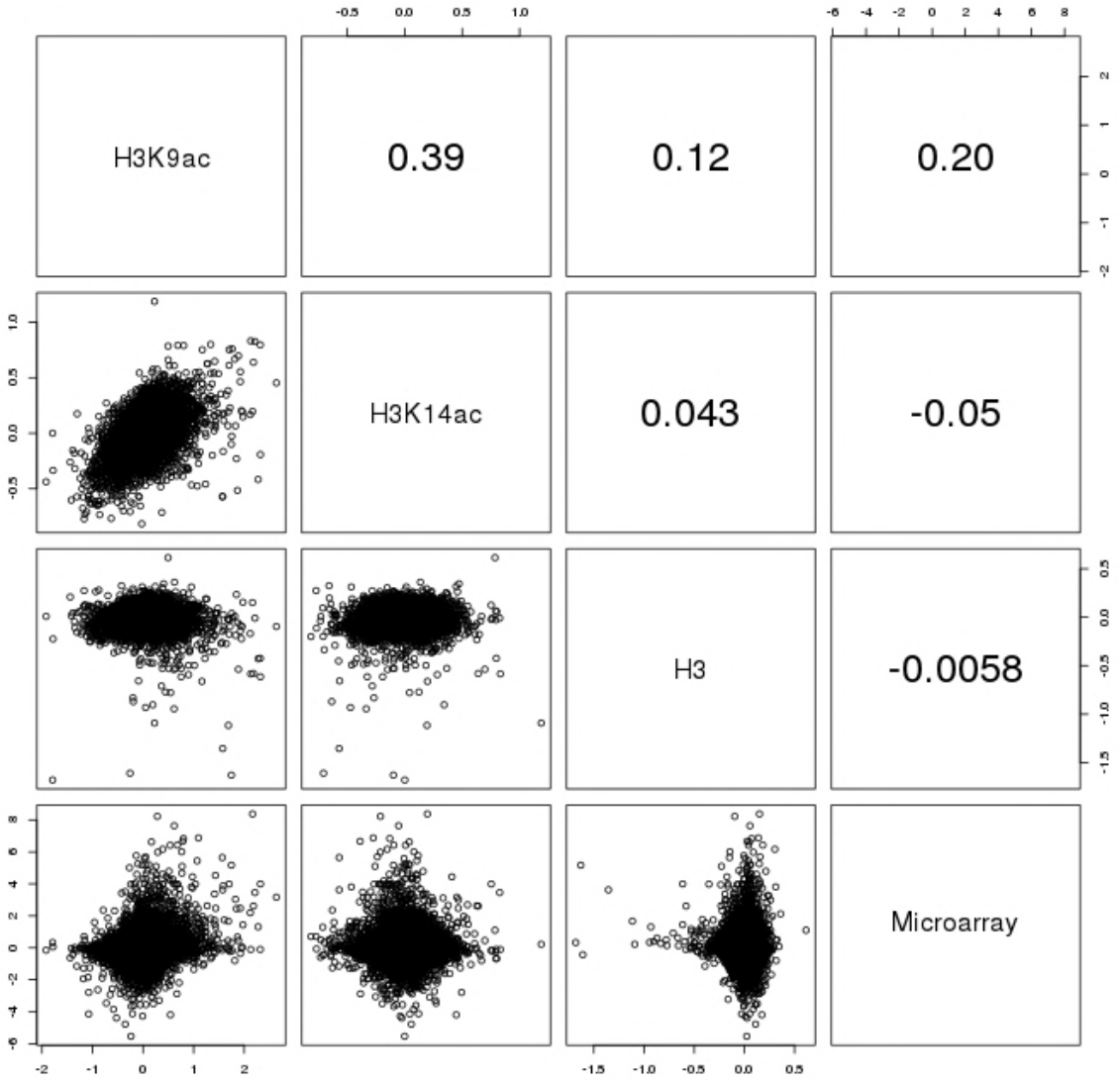

1132
1133 **Figure S1.**

1134

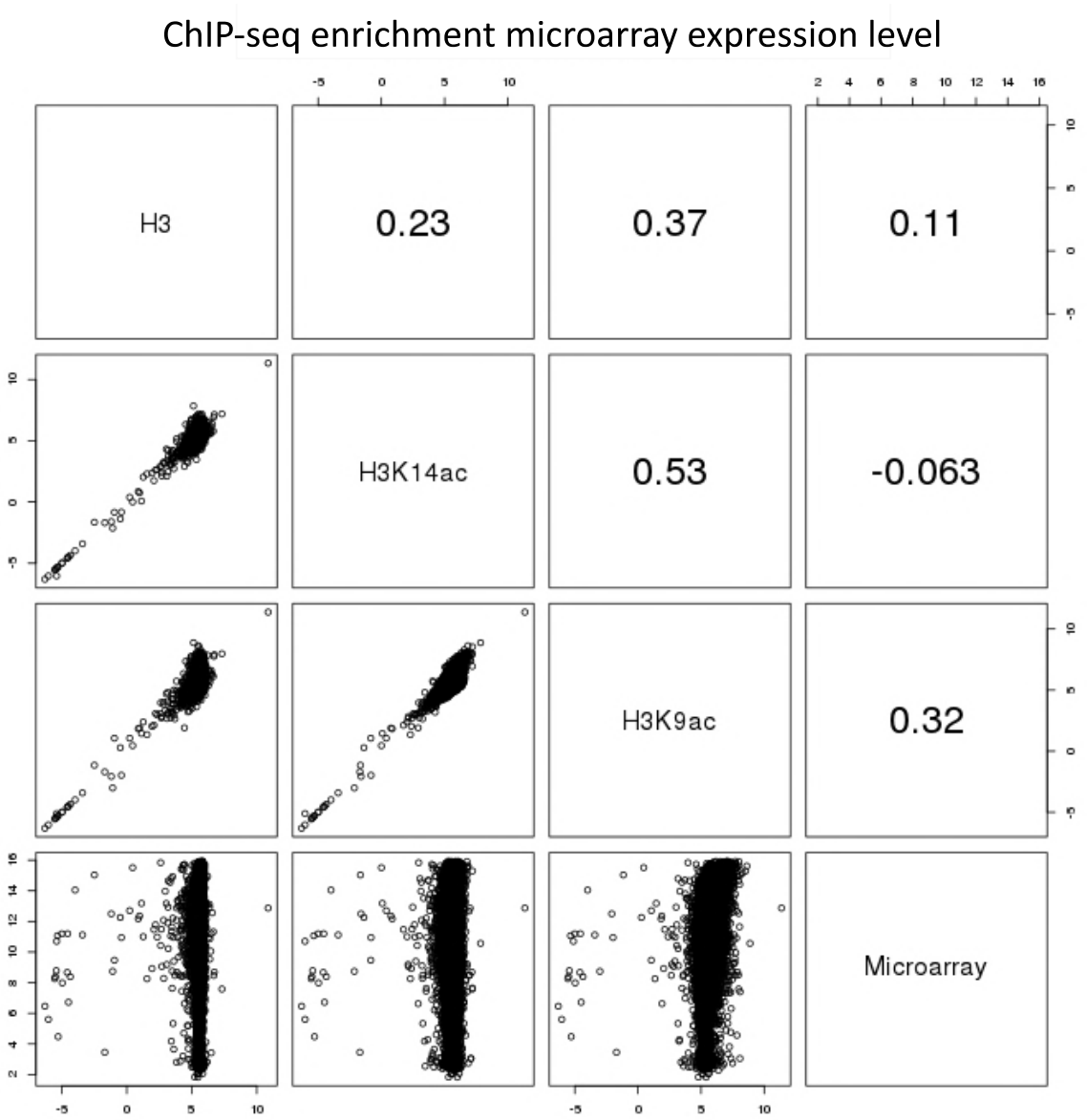

Figure S2.

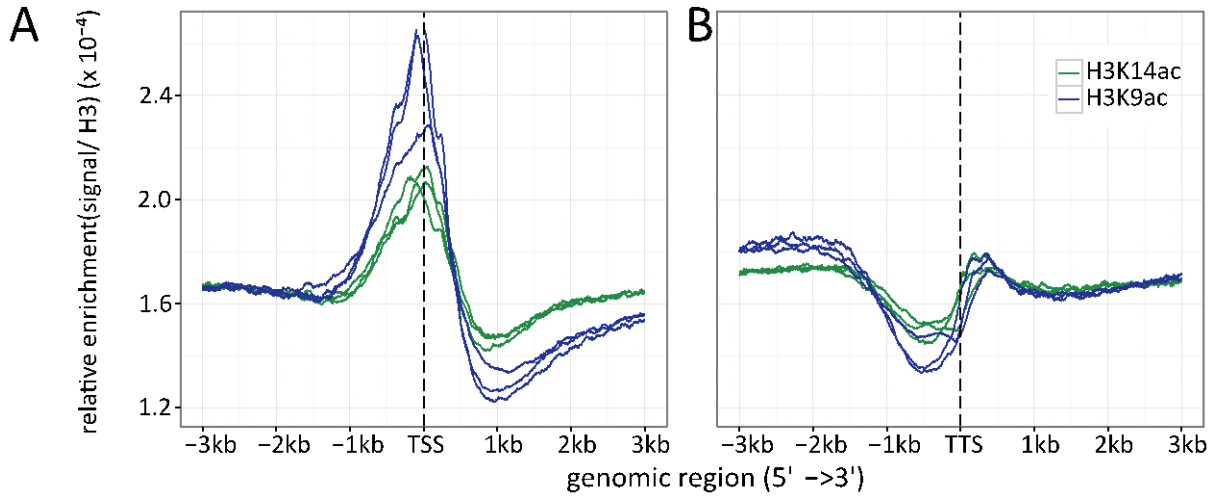

Figure S3.

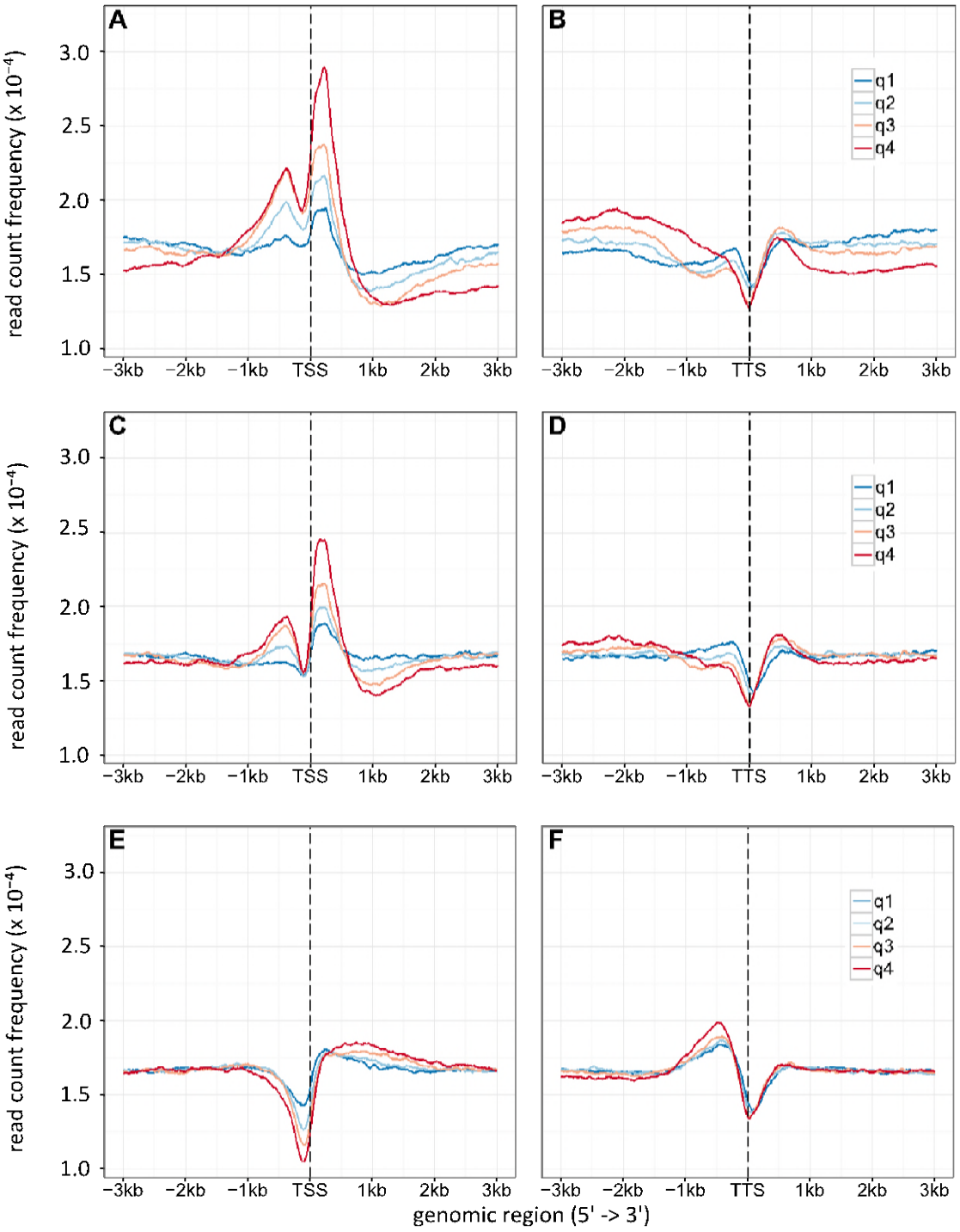

Figure S4.

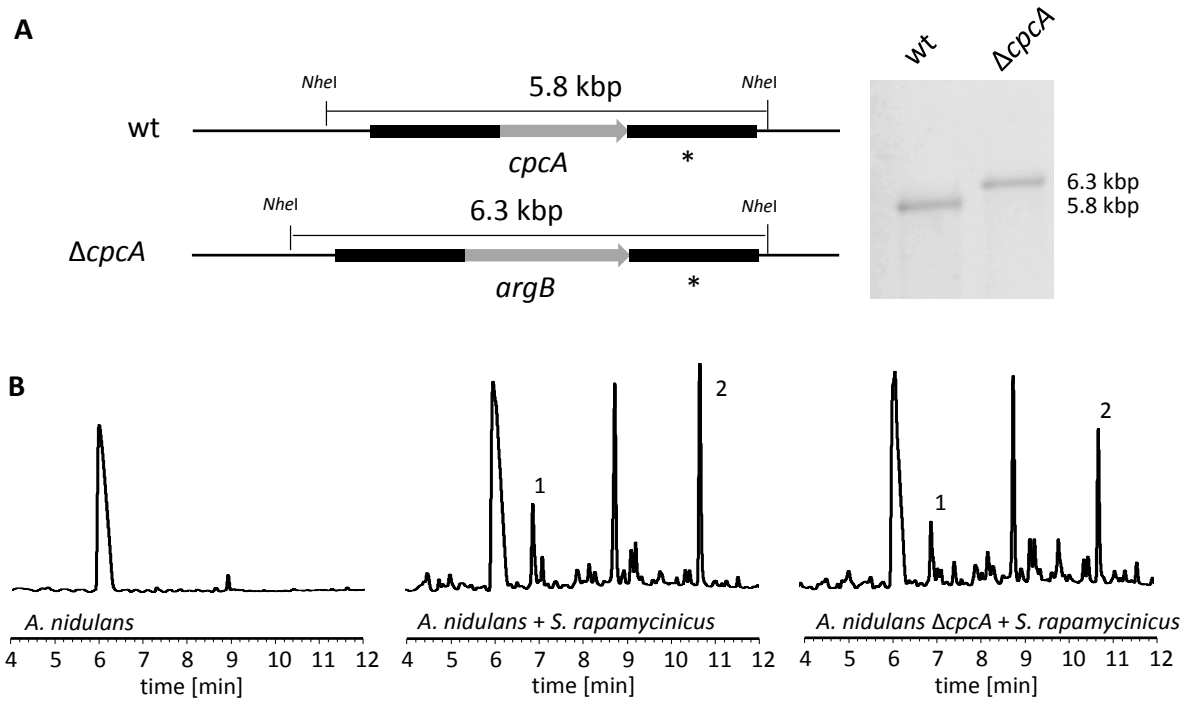

1146

1147 **Figure S5.**

1148

1149

1150

1151

1152

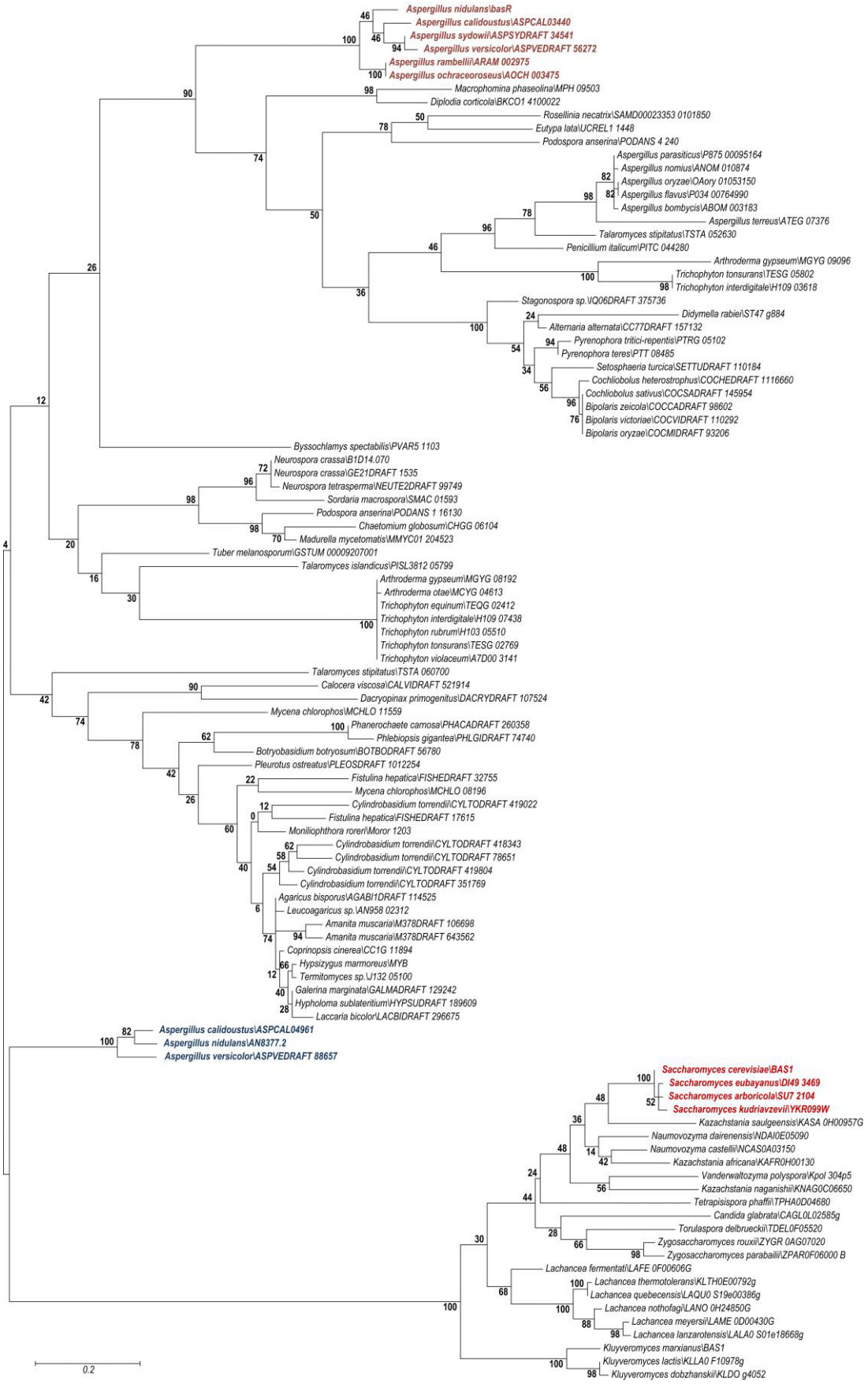

1153

1154 **Figure S6.**

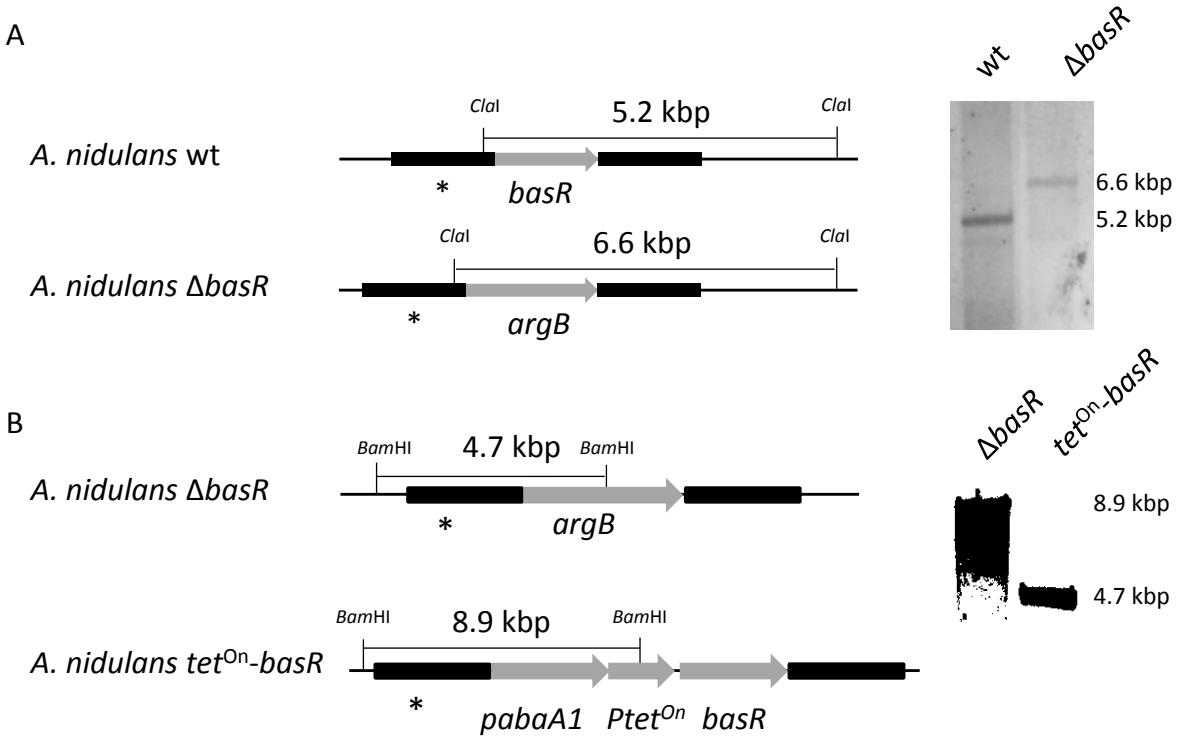

Figure S7.

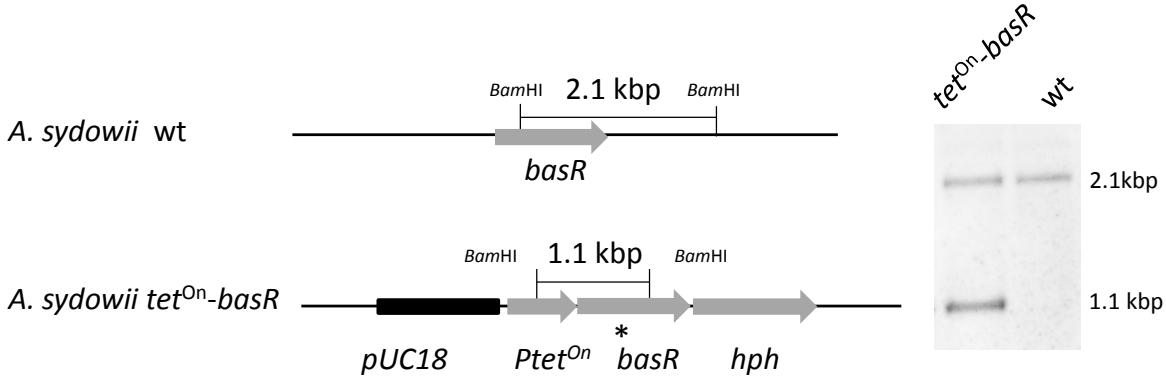

Figure S8.

Table S1. Summary of ChIP-seq data

Sample	**Mapping efficiency [%]**	**Total reads**	**Adaptor reads**	**Adaptor reads [%]**	**Unique reads**	**Unique reads [%]**	***A. nidulans* reads**	**Duplicate [%]**	**Trimmed Duplicate [%]**	***S. rapamycinicus* reads**	***A. nidulans* [%]**	***S. rapamycinicus* [%]**
25966_flagm2_rep2_rap_fastqc	83.65	6.740.753	2.049.874	30.4	2.499.561	37.3	112.408	11.565.627.824.421	116.738.263.092.368	3.507.733	16.68	52.04
25969_h3k9ac_rep1_fastqc	96.99	9.365.386	3.077.339	32.9	8.823.048	94.5	8.978.193	74.555.968.055.142	748.696.077.453.242	0.010012	95.87	0.11
25970_h3k9ac_rep1_rap_fastqc	96.64	7.737.559	2.493.774	32.2	673.711	87.2	6.624.136	762.365.916.062.742	764.078.025.056.828	0.768383	85.61	9.93
25973_h3k9ac_rep2_fastqc	98.3	7.541.067	2.408.844	31.9	7.202.729	96	7.339.192	766.193.983.227.339	768.284.051.621.336	0.004353	97.32	0.06
25974_h3k9ac_rep2_rap_fastqc	97.16	10.890.871	3.538.308	32.5	9.079.848	83.5	8.728.609	79.173.675.786.247	794.933.998.378.403	1.681.602	80.15	15.44
25977_h3k14ac_rep1_fastqc	97.99	4.975.966	1.603.206	32.2	4.781.717	96.1	4.862.224	901.966.216.764.041	89.927.577.136.475	0.001007	97.71	0.02
25978_h3k14ac_rep1_rap_fastqc	96.97	5.558.179	174.768	31.4	4.790.822	86.4	4.669.582	905.974.181.288.327	905.591.684.672.175	0.657575	84.01	11.83

25981_h3k14ac_rep2_fastqc	97.75	7.848.049	2.524.433	32.2	7.513.985	95.9	7.631.192	86.972.883.667.071	867.813.459.068.815	0.002981	97.24	0.04
25982_h3k14ac_rep2_rap_fastqc	97.25	5.365.781	1.707.664	31.8	4.754.462	88.6	4.684.201	929.740.213.555.733	928.976.176.425.656	0.492044	87.3	9.17
25985_h3cterm_rep1_fastqc	98.3	16.575.311	5.464.365	33	15.852.387	95.8	16.218.352	813.944.725.279.651	817.243.581.056.883	0.005381	97.85	0.03
25986_h3cterm_rep1_rap_fastqc	97.16	6.507.174	213.572	32.8	5.727.625	88.5	5.686.605	9.017.548.780.945	90.727.567.964.291	0.549903	87.39	8.45
25989_h3cterm_rep2_fastqc	97.93	7.211.698	2.378.043	33	6.807.968	95.3	6.965.766	875.255.935.788.041	882.069.230.353.478	0.00427	96.59	0.06
25990_h3cterm_rep2_rap_fastqc	97.64	12.234.444	4.041.382	33	10.561.374	86.7	10.366.001	863.349.575.870.974	869.220.274.291.627	139.243	84.73	11.38
25993_h3cterm_rep3_fastqc	97.65	22.793.994	7.367.013	32.3	21.685.933	95.1	22.177.124	690.901.496.209.322	692.369.343.128.389	0.010104	97.29	0.04
25994_h3cterm_rep3_rap_fastqc	97.59	15.631.595	4.989.982	31.9	1.360.676	87.1	13.412.004	794.449.484.478.621	796.526.289.875.721	1.706.112	85.8	10.91
25997_lane1_flagm2_wt_rap_fastqc	90.13	10.761.862	2.576.201	23.9	3.935.407	36.6	1.602.687	74.296.819.443.649	74.610.621.811.612	7.053.875	14.89	65.55
26003_h3k9ac_rep3_fastqc	97.76	16.902.561	5.398.124	31.9	16.124.992	95.5	16.435.405	694.896.967.502.731	696.871.654.676.839	0.013829	97.24	0.08

26004_h3k9ac_rep3_rap_fastqc	97.48	16.572.919	5.104.133	30.8	13.677.535	82.7	13.062.179	735.996.861.424.942	739.135.791.025.044	2.814.063	78.82	16.98
26007_h3k14ac_rep3_fastqc	97.89	14.574.983	474.023	32.5	13.939.149	95.7	14.156.851	779.406.442.069.405	781.452.414.804.995	0.040031	97.13	0.27
26008_h3k14ac_rep3_rap_fastqc	97.52	13.634.579	4.196.136	30.8	11.762.285	86.3	1.143.362	803.285.919.644.695	804.304.242.916.709	173.715	83.86	12.74
26011_lane2_flagm2_wt_rap_fastqc	89.83	8.022.504	1.969.244	24.5	3.022.492	37.7	134.348	788.149.626.049.476	791.792.240.473.135	5.094.587	16.75	63.5

1167 **Table S2.** List of primers used in this study.

Name	**Sequence (5'- 3')**
For generation of constructs for transformation of *A. nidulans*	
argB2for	ATGGGAGTCAAAGTTCTGTTTGC
argB2rev	GGAAGCGAGAGAACATGTCAA
basAlbfor	GCAGATCCAATGCCAGATGC
basAArgBlbrev	AACAGAACTTTGACTCCCATTATGAGGAGAAGATGATTATC
basAArgBrbfor	GACATGTTCTCTCGCTTCCGATTACTGTGATTATTGGCAGC
basArbrev	AGTTAAACATCAAGGACTTGGG
cpcAlbfor	GCGTTCTGGTGTCGGGTCTG
cpcAArgBlbrev	AACAGAACTTTGACTCCCATATGAAAAGAAAAATTCAGGG
cpcAArgBrbfor	GACATGTTCTCTCGCTTCCATCCTCTTTGACAGTTCGCTG
cpcArbrev	CGAGACACGGCATTCTGGCAC
NJ08	TGCCAGGGATAGAAACATGT
NJ09	CGCAGACCTTTCTACAGATCTGGCATATGAGGAGAAGATGATTATC
NJ10	TCCGGTTTCATACACCGGGCAAAGAATCTGGACATGCGACGGAG
NJ11	TCCATCTCAACTCCATCACATCACAATGACAGAACCTCGCCGG
NJ12	TACCTATGTCTAGTAAAAGGAT
NJ41	TTTACGGTGCACATGTTTCTATCCCTGGCACACNNNGTGTAGAAGATCTCCTACAATAT TCTCAGC
NJ42	CAAGAGCTATCCTTTTACTAGACATAGGTAAACTCGAGCCATCCGGAT
Pabacassfor	TGCCAGATCTGTAGAAAGGTC
TetONfor	TCTTTGCCCGGTGTATGAAACC
TetONrev	TGTGATGTGATGGAGTTGAGATGG
TetON_pUC18tailF	CACGACGTTGTAAAACGACGGCCAGTGCCATCTTTGCCCGGTGTATGAAA
Asyd_basRF	ATGGCTGAACAACGTCGGCG

Name	**Sequence (5'- 3')**
Asyd_basRR	TCAATATCCATACGACTGCC
poliC_basRsidtai	AGTTGTCCAGCGCCGACGTTGTTCAGCCATTGTGATGTGATGGAGTTGAG
Ttef_sydbastail_	CTCCAGAGAGGGCAGTCGTATGGATATTGAGCGGACATTCGATTTATGCC
hph_puc18tail_R	GATCCTCTAGAGTCGACCTGCAGGCATGCACTATTCCTTTGCCCTCGGAC
qRT-PCR	
Qacnfwd	CACCCTTGTTCTTGTTTTGCTC
Qacnrev	AAGTTCGCTTTGGCAACGC
qorsAfor	CTATACCACCGATAGCCAGGAC
qorsArev	CAGTGAGCAGGGCAAAGAAG
qorsDfor	GCAACGAGCCTGACATTACC
qorsDrev	CCGCACATCAACCATCTCTG
qareAfor	AAATCTAGCTCAGCGGCGAC
qareArev	GGGCTTTCCGCCATATCAAC
qniaDfor	CTGACGAAGGGGAGTGAAAG
qniaDrev	TCCATCCCAACGACAGTAGG
qprnDfor	CGCTTTTGGTCTGCGTTAC
qprnDrev	CCGCTCAAAAACCAGACAATC
qgdhAfor	TCAAGGGCATCATGGAGGAC
qgdhArev	CTTGGTGAAACCGGCAATG
qniiAfor	GCGGGAAGATGGCTGGATTTAC
qniiArev	CCACAGCTTCACCCTTCTTCAC
qtamAfor	TGATGACCAGCTCGTCAAAACC
Qtamrev	CCGCATCGTGCATACTTTCCTC
qgltAfor	GCCCGTAAGAATGTCAAGACCC

Name	**Sequence (5'- 3')**
qgltArev	GCTGAGAGCTGATGCCAGAAAG
qmeaAfor	TGACTACCTTGCCTGGACAC
qmeaArev	GCCGTTGCGATTCTTCCTTG
qureDfor	AGCGGGATGCAGCAAAGATG
qureDrev	AAGGCTCAACACTCCCAGAC
qprnBfor	GTCAGAGGTTGACATCTTTACG
qprnBrev	AAATCCACCACCAGACTCG
qbasRfw	GCGGGTACATGCCACAATAC
qbasRrev	TCTCGGGCATCATCAACTCC

1168